Noncanonical thyroid hormone signaling mediates cardiometabolic effects in vivo

G. Sebastian Hönes[a], Helena Rakov[a], John Logan[b], Xiao-Hui Liao[c], Eugenie Werbenko[b], Andrea S. Pollard[b], Stine M. Præstholm[d], Majken S. Siersbæk[d], Eddy Rijntjes[e], Janina Gassen[a], Sören Latteyer[a], Kathrin Engels[a], Karl-Heinz Strucksberg[a], Petra Kleinbongard[f], Denise Zwanziger[a], Jan Rozman[g,h], Valerie Gailus-Durner[g], Helmut Fuchs[g], Martin Hrabe de Angelis[g,h,i], Ludger Klein-Hitpass[j], Josef Köhrle[e], David L. Armstrong[k], Lars Grøntved[d], J. H. Duncan Bassett[b], Graham R. Williams[b], Samuel Refetoff[c,l,m], Dagmar Führer[a], and Lars C. Moeller[a,1]

[a]Department of Endocrinology, Diabetes and Metabolism, University Hospital Essen, University of Duisburg-Essen, 45147 Essen, Germany; [b]Molecular Endocrinology Laboratory, Department of Medicine, Imperial College London, London W12 0NN, United Kingdom; [c]Department of Medicine, The University of Chicago, Chicago, IL 60637; [d]Department of Biochemistry and Molecular Biology, University of Southern Denmark, 5230 Odense, Denmark; [e]Charité-Universitätsmedizin Berlin, Corporate Member of Freie Universität Berlin, Humboldt-Universität zu Berlin, and Berlin Institute of Health, Institut für Experimentelle Endokrinologie, 10117 Berlin, Germany; [f]Institute for Pathophysiology, West-German Heart and Vascular Center Essen, University Hospital Essen, University of Duisburg-Essen, 45147 Essen, Germany; [g]German Mouse Clinic, Institute of Experimental Genetics, Helmholtz Zentrum München, German Research Center for Environmental Health, 85764 Neuherberg, Germany; [h]German Center for Diabetes Research, 85764 Neuherberg, Germany; [i]Chair of Experimental Genetics, School of Life Science Weihenstephan, Technische Universität München, 85354 Freising, Germany; [j]Institute of Cell Biology (Cancer Research), Faculty of Medicine, University of Duisburg-Essen, 45147 Essen, Germany; [k]Laboratory of Neurobiology, National Institute of Environmental Health and Sciences, National Institutes of Health, Research Triangle Park, NC 27709; [l]Department of Pediatrics, The University of Chicago, Chicago, IL 60637; and [m]Committee on Genetics, The University of Chicago, Chicago, IL 60637

Edited by David W. Russell, University of Texas Southwestern Medical Center, Dallas, TX, and approved November 15, 2017 (received for review April 25, 2017)

Thyroid hormone (TH) and TH receptors (TRs) α and β act by binding to TH response elements (TREs) in regulatory regions of target genes. This nuclear signaling is established as the canonical or type 1 pathway for TH action. Nevertheless, TRs also rapidly activate intracellular second-messenger signaling pathways independently of gene expression (noncanonical or type 3 TR signaling). To test the physiological relevance of noncanonical TR signaling, we generated knockin mice with a mutation in the TR DNA-binding domain that abrogates binding to DNA and leads to complete loss of canonical TH action. We show that several important physiological TH effects are preserved despite the disruption of DNA binding of TRα and TRβ, most notably heart rate, body temperature, blood glucose, and triglyceride concentration, all of which were regulated by noncanonical TR signaling. Additionally, we confirm that TRE-binding–defective TRβ leads to disruption of the hypothalamic–pituitary–thyroid axis with resistance to TH, while mutation of TRα causes a severe delay in skeletal development, thus demonstrating tissue- and TR isoform-specific canonical signaling. These findings provide in vivo evidence that noncanonical TR signaling exerts physiologically important cardiometabolic effects that are distinct from canonical actions. These data challenge the current paradigm that in vivo physiological TH action is mediated exclusively via regulation of gene transcription at the nuclear level.

thyroid hormone receptor | noncanonical signaling | thyroid hormone action | skeleton | cardiometabolic effects

Thyroid hormone (TH) plays an essential role in organ development and metabolic homeostasis. The effects of 3,3′,5-triiodo-L-thyronine (T_3), the active TH, are mediated by TH receptors (TRs) α and β. Canonical TR signaling controls gene expression in the nucleus directly. This mechanism was recently classified as type 1 TR-dependent TH signaling (Fig. 1*A*) (1): TRs bind to thyroid hormone response elements (TREs) in regulatory regions of target genes. In the absence of T_3, TRs recruit corepressors with histone deacetylase activity, preventing transcription. T_3 binding to TRs causes the release of corepressors, which are replaced by coactivators that engage histone acetylases and RNA polymerase II to activate gene transcription (2, 3). Thus, TRs act as hormone-dependent transcription factors. Consequently, the current paradigm of TH action attributes its physiological effects to the genes directly regulated via canonical TR signaling on DNA.

Beyond that, additional and distinct mechanisms of TR signaling have been demonstrated. T_3 and TRβ can modulate intracellular second messenger signaling, e.g., the PI3K pathway (TR-dependent signaling of TH without DNA binding, type 3) (1, 4–7). A specific molecular mechanism for PI3K activation by TRβ has been identified and demonstrated to be essential for normal synapse development and plasticity in mice by mutating a specific tyrosine residue to phenylalanine in TRβ (7). Noncanonical signaling by TRα remains ill-defined, and its physiological importance is unknown. Such non-type 1 TH/TR action is considered noncanonical, because it is independent of DNA binding and TRE binding, does not require gene transcription or protein synthesis as the initial event, and may, therefore, also be more rapid (Fig. 1*B*).

Significance

This study changes our understanding of how thyroid hormone acts. Thyroid hormone receptors are considered typical nuclear receptors that bind to DNA and, after binding, alter the expression of their target genes and regulate physiological responses. Nevertheless, we show that thyroid hormone still mediates important physiological effects in mice expressing mutant receptors that cannot bind DNA. These are predominantly linked to energy metabolism and include glucose and triglyceride concentrations, body temperature, locomotor activity, and heart rate. This study provides in vivo evidence that thyroid hormone receptors mediate physiologically relevant effects that are independent of DNA binding and direct activation of gene expression.

Author contributions: G.S.H. and L.C.M. designed research; G.S.H., H.R., J.L., X.-H.L., E.W., A.S.P., S.M.P., M.S.S., E.R., J.G., S.L., K.E., K.-H.S., D.Z., J.R., V.G.-D., H.F., M.H.d.A., L.K.-H., L.G., and L.C.M. performed research; S.M.P., M.S.S., P.K., J.R., V.G.-D., H.F., M.H.d.A., L.K.-H., J.K., D.L.A., L.G., J.H.D.B., G.R.W., and S.R. contributed new reagents/analytic tools; G.S.H., S.M.P., M.S.S., J.R., V.G.-D., H.F., M.H.d.A., L.K.-H., J.K., L.G., J.H.D.B., G.R.W., S.R., D.F., and L.C.M. analyzed data; and G.S.H., J.H.D.B., G.R.W., and L.C.M. wrote the paper.

The authors declare no conflict of interest.

This article is a PNAS Direct Submission.

Data deposition: Data have been deposited in the National Center for Biotechnology Information Gene Expression Omnibus database (accession nos. GSE93864 for microarray data and GSE104877 for H3K27 ChIP-seq Illumina sequencing).

[1]To whom correspondence should be addressed. Email: lars.moeller@uni-due.de.

This article contains supporting information online at www.pnas.org/lookup/suppl/doi:10.1073/pnas.1706801115/-/DCSupplemental.

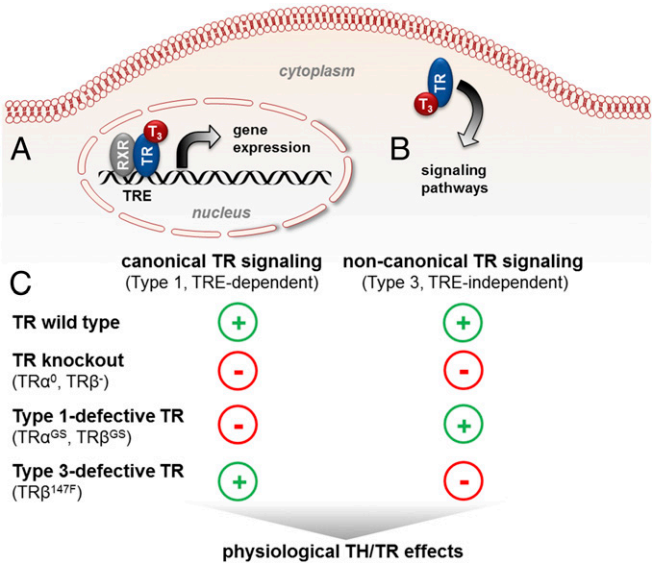

Fig. 1. Canonical and noncanonical TR signaling. (*A*) Canonical TR signaling requires binding of TR to regulatory DNA sequences, the TREs, mostly as a heterodimer with RXR. Binding of T_3 leads to an exchange of cofactors that initiates or represses the transcription of the target genes. (*B*) Noncanonical action of TRs involves rapid activation of signaling pathways without DNA binding. (*C*) Present (+) and absent (–) TR signaling in mouse models. In TR-WT mice, the TR can mediate both canonical and noncanonical signaling. In TR-KO mice, both effects are absent. In mice with TRE-binding–deficient TRs, canonical signaling is abolished, and only noncanonical signaling is preserved. Conversely, in mice with selective abrogation of PI3K signaling, this noncanonical TH effect is missing, while canonical signaling is preserved. Thus, a comparison of these mice can determine whether the signaling mechanism responsible for TH effects is canonical or noncanonical and PI3K mediated.

To determine the physiological consequences of noncanonical TH/TR action in vivo, we generated $TR\alpha^{GS}$ and $TR\beta^{GS}$ mice that lack canonical TR signaling by replacing glutamic acid (E) and glycine (G) in the first zinc finger of the DNA-binding domain of TRα and TRβ with glycine and serine (S). This GS mutation severely impairs TR binding to TREs and abrogates canonical TR signaling (8, 9). Since TRE binding is abolished, only the noncanonical TH actions are preserved in TR-GS–mutant mice. By contrast, the TR can mediate both canonical and noncanonical actions of TH in WT mice, whereas both actions are absent in TR-KO mice (Fig. 1*C*).

Therefore we hypothesized that a comparison of WT, TR-KO, and TR-GS mice would determine whether canonical or noncanonical TR signaling underlies physiological TH responses. A phenotypic difference between WT and TR-KO mice and similarity of TR-KO and TR-GS mice would indicate that canonical TR signaling is required for a particular phenotype (Fig. 1*C*). Conversely, if a phenotype is concordant between TR-GS and WT mice but discordant from TR-KO mice, then only noncanonical signaling would be required.

We also included $TR\beta^{147F}$ mice, in which tyrosine 147 of TRβ is changed to phenylalanine (Y147F), as an additional control for TRβ signaling. Tyrosine 147 is crucial for TRβ-mediated activation of PI3K, and replacement by phenylalanine abrogates PI3K activation. Nevertheless, the classical TRE-mediated actions of TRβ are unaffected in $TR\beta^{147F}$ mice (7). Thus, the $TR\beta^{147F}$ mice are a specific negative control for noncanonical, PI3K-mediated TH/TRβ effects, as TRβ-mediated PI3K signaling is absent in these mice (Fig. 1*C*).

Here we provide in vivo evidence that noncanonical TR signaling is physiologically important and contributes significantly to TH action, specifically for the regulation of body temperature, oxygen consumption (VO_2), locomotor activity, heart rate, and triglyceride and glucose concentrations, important parameters of cardiometabolic homeostasis and energy balance.

Results

The GS Mutation Abrogates Canonical TR Signaling in Vitro and in Vivo. Canonical TR signaling consists of TR binding to TREs in the regulatory regions of target genes and subsequent activation of gene expression. ChIP-sequencing (ChIP-seq) analyses in mouse liver reported a DR+4 motif, a direct repeat of two 5′-AGGTCA-3′ half-sites in the same orientation separated by four nucleotides, as the most prevalent TRE in T_3-induced genes (10–12). This consensus DR+4 TRE was used in a fluorescent EMSA to test DNA binding affinity of the TRα and TRβ variants (TRβ, TRβ125GS, TRβY147F, TRα, and TRα71GS). Only TRβ, TRβY147F, and TRα bound to the DR+4 probe; the TRβ125GS and TRα71GS receptors did not (Fig. 2*A*). The GS mutation abrogated DNA binding of both TRα and TRβ. Next, we tested the transcriptional activity of TRα71GS, TRβ125GS, and TRβY147F mutants in vitro using a TH-responsive luciferase reporter plasmid (DR+4-TKLuc) in comparison with WT TRs. Empty vector and TR mutants TRαG291R and TRβG345R served as controls. These mutant TRs cannot bind T_3 and cannot activate gene transcription after T_3 treatment (13). T_3 increased luciferase activity eightfold with WT TRα, TRβ, and TRβY147F but not with empty vector or TRβG345R and TRαG291R (Fig. 2*B*). Luciferase activity was not increased by T_3 with the TRα71GS and TRβ125GS mutants, demonstrating in vitro that the GS mutation in the DNA-binding domain abolishes the canonical TRE-mediated transcriptional activity of TRα and TRβ. This was confirmed by experiments with a common variant of the 3′ half-site (AGGACA) (Fig. S1 *A* and *B*).

To abolish the canonical TR action in vivo, we introduced the GS mutation into the murine WT *Thra* and *Thrb* gene loci, generating $TR\alpha^{GS}$ ($Thra^{GS/GS}$) and $TR\beta^{GS}$ ($Thrb^{GS/GS}$) mice. We determined the expression of known TH-responsive genes in these mice in comparison with WT and the respective TR-KO mice ($TR\alpha^0$ and $TR\beta^-$ mice; genotypes are $Thra^{0/0}$ and $Thrb^{-/-}$, respectively). As TRα is predominantly expressed in heart and TRβ in liver, we studied these two tissues. In heart, expression of *Myh6* and *Myh7* mRNAs in $TR\alpha^{GS}$ mice differed significantly from their expression in WT mice and was comparable to that in $TR\alpha^0$ mice (Fig. 3*A*), demonstrating that the GS mutation in TRα abrogates canonical TH/TRα action in vivo. For TRβ-mutant mice, the different systemic TH concentrations in WT, $TR\beta^{GS}$, and $TR\beta^-$ mice had to be equalized. Thus, we determined TH-induced gene expression in hypothyroid animals without and with T_3 treatment. In livers of WT mice, T_3 induced expression of *Dio1*, *Spot14*, *Me1*, and *Bcl3* mRNAs (Fig. 3*B* and Fig. S1 *C* and *D*). This induction was equally reduced in both $TR\beta^-$ mice and $TR\beta^{GS}$ mice, demonstrating that the GS mutation in TRβ has the same effect on canonical TH/TR-mediated gene expression as the complete absence of TRβ in $TR\beta^-$ mice.

To evaluate recruitment of TRβ mutants to DNA, we performed ChIP against TRβ and its heterodimerization partner retinoid X receptor alpha (RXRα) in liver tissue from T_3-treated animals and evaluated the occupancy of known TR-binding sites previously identified in mouse liver tissue, e.g., in the *Dio1*, *NcoR2*, *H13*, and *Strbp* genes (Fig. 3*C* and Fig. S1*E*). Both WT and the $TR\beta^{147F}$ mutant occupy these TR-binding sites together with RXRα, whereas the $TR\beta^{GS}$ mutant and $TR\beta^-$ show little or no enrichment, confirming that the GS mutation in the DNA-binding domain of TRβ disrupts TRβ's interaction with chromatin. Moreover, evaluation of histone 3 lysine 27 acetylation (H3K27Ac) at these binding sites showed that impaired occupancy with TRβ in $TR\beta^-$ and $TR\beta^{GS}$ mice results in reduced histone acetylation (Fig. 3*C* and Fig. S1*E*). To evaluate the effect on histone acetylation genome-wide, we performed ChIP-seq against H3K27Ac in the liver of hypo- and T_3-treated hyperthyroid WT and TRβ mutant animals.

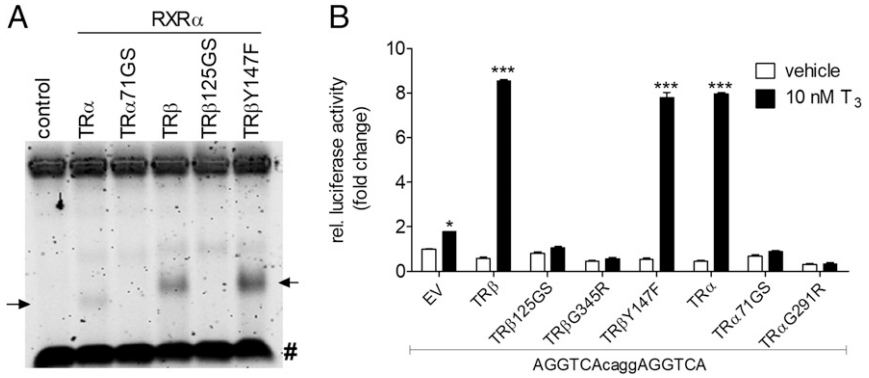

Fig. 2. The GS mutation abolishes TR binding to DNA and canonical TR signaling in vitro. (*A*) Fluorescent EMSA was performed with 4 μL of reticulocyte-translated TRαWT, TRα71GS, TRβWT, TRβ125GS, and TRβY147F and 2 μL of RXRα on a 5′-Cy5–labeled DR+4 TRE probe. Arrows indicate bands of TRα and TRβ binding to probe; #, free probe. (*B*) HEK293 cells transfected with plasmids encoding for TRβ, TRβ125GS, TRβY147F, TRα, and TRα71GS and a DR+4-luciferase reporter plasmid. Empty vector (EV) and TR mutants without T_3 binding (TRαG291R and TRβG345R) served as negative controls. Cells were treated with vehicle (open bars) or with 10 nM T_3 for 48 h to induce luciferase expression via canonical TR/TRE-mediated action for TRα and TRβ variants (black bars); $n = 3$. Data are shown as mean ± SEM; ANOVA and Tukey's post hoc test; $^*P < 0.05$; $^{***}P < 0.001$.

Sequenced tags were quantified at all previously identified DNase-accessible regions (12), and we identified more than 500 regions where H3K27Ac was differently regulated by T_3 in WT animals (Fig. S1*F*). We quantified H3K27Ac at these differentially regulated regions in liver samples from hypo- and T_3-treated hyperthyroid WT and TRβ$^-$ animals and animals carrying the GS and 147F TRβ mutants. Hierarchical clustering revealed that T_3-induced H3K27Ac in animals with the 147F mutation is very similar to that observed in WT animals. By contrast, the TRβGS mutation or TRβ deletion resulted in attenuated H3K27Ac after T_3 treatment (Fig. 3*D*). Consistent with this, H3K27Ac is increased in response to T_3 at previously identified TR-binding sites in the *Dio1* gene loci in WT and TRβ^{147F} mice but not in TRβ^{GS} or TRβ$^-$ animals (Fig. 3*E*).

We then used transcriptome analysis to determine whether TRβ125GS and TRβ147F mutants possess residual transcriptional activity affecting known target genes or had acquired new target-gene specificity. Hypothyroid WT, TRβ$^-$, TRβ^{GS}, and TRβ^{147F} mice were treated with a single dose of T_3, and hepatic gene expression was determined after 6 h by microarray analysis. Fig. 3*F* shows the results in a dendrogram with mice grouped by similarity of their gene-expression patterns, not by genotype. The gene-expression patterns in WT and TRβ^{147F} mice were clearly different from those in TRβ$^-$ and TRβ^{GS} mice and formed their own branch in the hypothyroid and T_3-treatment groups. Importantly, TRβ$^-$ and TRβ^{GS} mice were grouped together because of the similarity of their hepatic gene-expression patterns. In fact, T_3-treated TRβ$^-$ and TRβ^{GS} mice could not be distinguished by gene-expression pattern. Thus, the GS mutation renders the TR transcriptionally nonfunctional in vivo.

Regulation of the Hypothalamic–Pituitary–Thyroid Axis Requires Canonical TRβ Signaling. TH production and secretion is regulated by the hypothalamic–pituitary–thyroid (HPT) axis negative-feedback loop. Inhibition of thyroid-stimulating hormone (TSH) is mediated by TRβ (14–16) and depends on DNA binding of TRβ (9). In accordance with these reports, basal serum TSH was significantly higher in TRβ$^-$ and TRβ^{GS} mice than in WT mice (Fig. 4*A*). As a consequence of elevated TSH, serum thyroxine (T_4) and T_3 concentrations were also significantly higher in TRβ$^-$ and TRβ^{GS} mice than in WT mice (Fig. 4*B* and Fig. S2*A*). The combination of elevated circulating TH concentrations and elevated TSH demonstrates central resistance to TH due to the lack of the receptor in TRβ$^-$ mice and, importantly, a corresponding absence of canonical TRβ action in the HPT axis of TRβ^{GS} mice. In TRβ^{147F} mice with intact DNA binding and canonical signaling, serum T_3 and T_4 concentrations and pituitary TSHβ expression were normal (7). TSH, T_4, and T_3 concentrations in TRα^0 mice (devoid of TRα1 and TRα2) and TRα^{GS} mice were not different from those in WT mice (Fig. 4 *A* and *B* and Fig. S2*A*).

Skeletal Development Requires Canonical TRα Signaling. We measured growth curves from WT, TRα^0, TRα^{GS}, TRβ$^-$, and TRβ^{GS} mice. Growth curves of TRβ$^-$ and TRβ^{GS} mice were not different from those of WT mice (Fig. S2 *B* and *C*). However, TRα^0 and TRα^{GS} mice had a similar delay in linear growth and gain in body weight (BW) compared with WT mice (Fig. 4 *C*–*F*). To investigate the underlying cause, skeletal analysis of TRα^0 and TRα^{GS} mice was performed after weaning at postnatal day 21 (P21). X-ray microradiography revealed a similar decrease in bone length and vertebral height in TRα^{GS} and TRα^0 mice, together with a reduction in bone mineral content in vertebrae but no difference in long bones (Fig. 5*A* and Fig. S3). Histological analysis of the growth plate revealed a delay in endochondral ossification similarly affecting both TRα^{GS} and TRα^0 mice (Fig. 5*B*). This delay comprised a decrease in the size of the secondary ossification center together with an increase in the reserve zone width and a decrease in the hypertrophic zone, features that are characteristic of impaired T_3 action (17, 18). High-resolution micro-computed tomography (micro-CT) imaging demonstrated epiphyseal dysgenesis, increased trabecular bone mass, and reduced metaphyseal inwaisting consistent with a bone-modeling defect and delayed endochondral ossification (Fig. 5 *C* and *D*). These are all classic features of impaired T_3 action in bone (18, 19). In summary, these data demonstrate an equivalent delay in skeletal development due to similar loss of TRE-mediated canonical TRα signaling in TRα^0 and TRα^{GS} mice. These findings establish that T_3 actions in the skeleton are mediated by canonical actions of TRα on TREs.

Noncanonical TRβ Action Decreases Blood Glucose Concentration. T_3 treatment has been shown to reduce serum glucose concentration rapidly in lean and obese mice (20). We hypothesized that such a rapid TH effect could be mediated noncanonically by TRs and thus be present in WT and in TRα^{GS} and TRβ^{GS} mice. We tested this hypothesis first in WT, TRβ$^-$, TRβ^{GS}, and TRβ^{147F} mice. Basal serum glucose after 1 h of fasting was not different among the TRβ genotypes (Table S1). T_3 injection rapidly decreased blood glucose within 60 min in WT mice (Fig. 6*A* and Table S1). Strikingly, this hypoglycemic effect of T_3 was abolished in TRβ$^-$ mice but was fully preserved in TRβ^{GS} mice. We conclude that the decrease in blood glucose after T_3 treatment is mediated by TRβ, as it is absent in TRβ$^-$ mice. The similar decrease in blood glucose

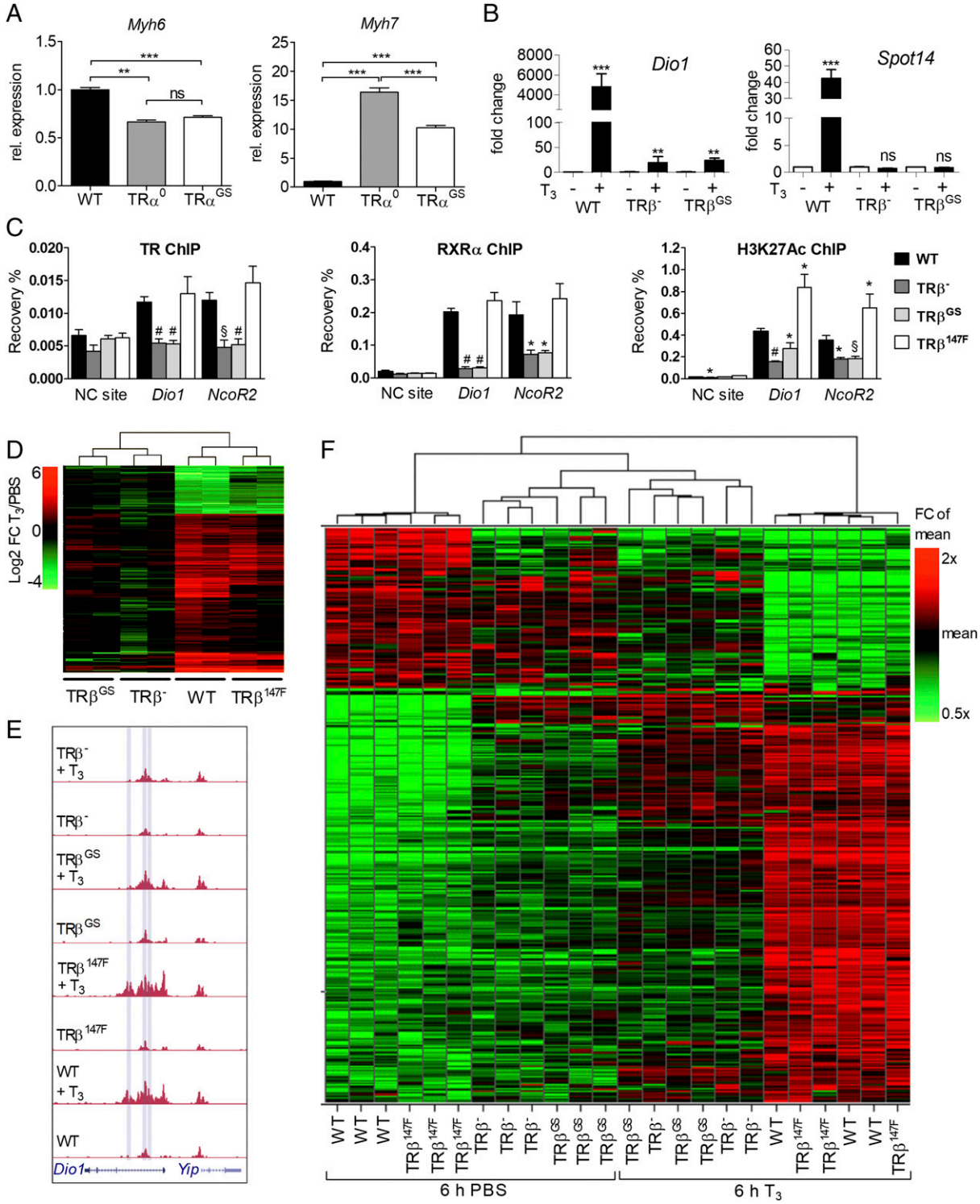

Fig. 3. The GS mutation abolishes TR binding to DNA and canonical TR signaling in vivo. (*A*) Relative expression of *Myh6* and *Myh7* in hearts of male WT (black bars), $TR\alpha^0$ (gray bars), and $TR\alpha^{GS}$ (open bars) mice; $n = 6$. Data are shown as mean ± SEM; ANOVA and Tukey's post hoc test; ns, not significant, $^{**}P < 0.01$, $^{***}P < 0.001$. (*B*) Response of TH target genes (*Dio1* and *Spot14*) to T_3 in livers of hypothyroid WT, $TR\beta^-$, and $TR\beta^{GS}$ mice. Hypothyroid mice were injected either with vehicle (open bars) or with 50 ng/g BW T_3 (black bars) for four consecutive days; $n = 6$ mice per genotype. Data are shown as mean ± SEM; ANOVA and Tukey's post hoc test; ns, not significant, $^{**}P < 0.01$; $^{***}P < 0.001$. (*C*) ChIP of TRβ, RXRα, and H3K27Ac was followed by qPCR to determine H3K27 acetylation and recruitment of RXRα and TR to TR-binding sites located +7.0 kb and +22.4 kb from the transcriptional start site of *Dio1* and *NcoR2*, respectively, in T_3-treated $TR\beta^{147F}$, $TR\beta^-$, and $TR\beta^{GS}$ mice compared with WT mice; $n = 4$–6. Data are shown as mean ± SEM; Student's *t* test; $^*P < 0.05$; $^{\#}P < 0.005$; $^{\S}P < 0.001$; NC, negative control. (*D*) H3K27Ac ChIP-seq experiments were performed using livers from hypothyroid WT mice treated with PBS or T_3 for 6 h. A heatmap illustrates log2 fold change of H3K27Ac comparing T_3 treatment with PBS for all genotypes at 537 DNase-accessible regions with differential H3K27Ac calculated by DEseq2 (Bioconductor). (*E*) University of California, Santa Cruz Genome browser tracks of H3K27Ac enrichment profiles at the *Dio1* gene locus for all four genotypes injected with PBS or T_3. Vertical blue bars mark TR-binding sites. (*F*) Hierarchical clustering of gene-expression data (microarray) from livers of hypothyroid WT, $TR\beta^-$, $TR\beta^{GS}$, and $TR\beta^{147F}$ mice treated with either 200 ng/g BW T_3 or PBS for 6 h ($n = 3$).

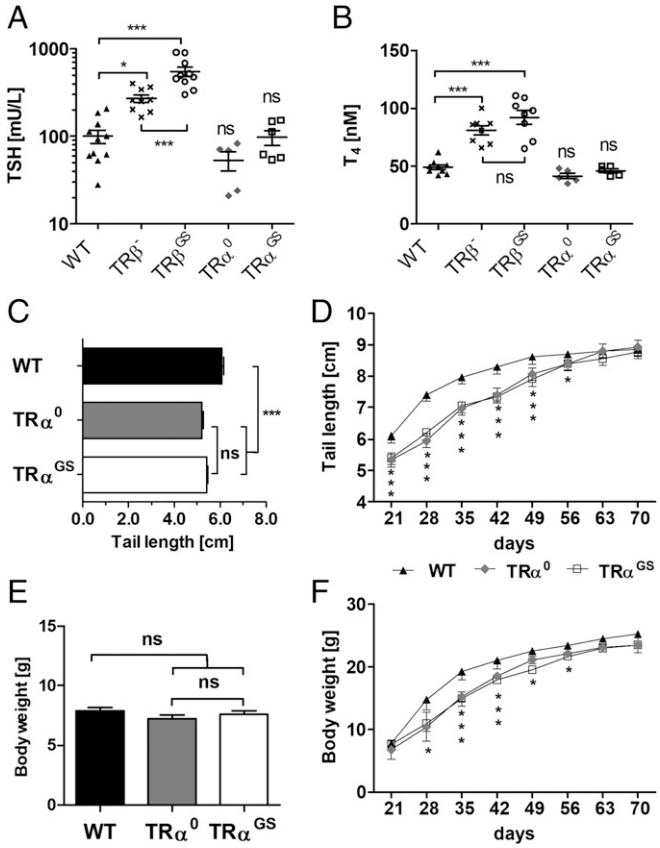

Fig. 4. Canonical TR action is required for TSH repression and normal growth. (*A* and *B*) TSH (*A*) and T_4 (*B*) in serum of 15-wk-old WT (black triangles; $n = 11$) TRβ$^-$ (x; $n = 9$), TRβ^{GS} (open circles; $n = 10$), TRα^0 (gray diamonds; $n = 5$), and TRα^{GS} (open squares; $n = 6$) male mice. Data are shown as mean ± SEM; ANOVA and Tukey's post hoc test; $^*P < 0.05$; $^{***}P < 0.001$; ns, not significant. (*C*) Tail length of 21-d-old WT (black bar), TRα^0 (gray bar), and TRα^{GS} (open bar) mice. (*D*) Linear growth was recorded until the age of 70 d. (*E* and *F*) Bodyweight on P21 (*E*) and recorded until the age of 70 d (*F*); $n = 6$; mean ± SD for tail length and BW at P21 and follow-up; ANOVA and Tukey's post hoc test; ns, not significant; $^*P < 0.05$; $^{***}P < 0.001$.

seen in both WT and TRβ^{GS} mice demonstrates that this effect is mediated by noncanonical TRβ signaling. Furthermore, this effect occurs within 60 min, which is likely too rapid to be dependent on RNA transcription and new protein translation. This conclusion is further supported by the failure of T_3 to induce hypoglycemia in TRβ^{147F} mice, which also demonstrates that PI3K activation by TRβ is required to lower the glucose concentration. By contrast, TRα is not involved in hypoglycemic response to T_3, as it is unable to compensate for the lack of TRβ in TRβ$^-$ mice.

Noncanonical TRβ Signaling Maintains Normal Serum and Liver Triglyceride Concentration. Serum triglyceride concentration is under TH control (21, 22). Previous studies have shown elevated serum triglyceride concentration in TRβ knockin mice with resistance to TH (TRβ^{PV}), indicating that TRβ mediates TH regulation of triglycerides (23). We therefore measured serum triglyceride concentrations in untreated WT, TRβ$^-$, TRβ^{GS}, and TR^{β147F} mice. Triglyceride concentrations were significantly higher in TRβ$^-$ and TRβ^{147F} mice than in WT mice (300 ± 61 and 264 ± 26 vs. 152 ± 23 mg/dL; $P < 0.05$) but not in TRβ^{GS} mice (123 ± 34 mg/dL; n.s.) (Fig. 6*B*). Cholesterol, albumin, and total protein concentrations were not different among WT, TRβ$^-$, TRβ^{GS}, and TRβ^{147F} mice (Table S2). These results demonstrate that in the absence of noncanonical TRβ action the serum triglyceride concentration is elevated in TRβ$^-$ and TRβ^{147F} mice. A possible explanation for increased serum triglyceride concentration was increased triglyceride synthesis in the liver. Compared with WT mice, the expression of several key enzymes involved in triglyceride synthesis (Scd1, Me1, Fasn) was increased in livers of TRβ$^-$ and TRβ^{147F} mice but was not increased or was increased to a lesser extent in TRβ^{GS} mice (Fig. 6 *C* and *E* and Fig. S4). Accordingly, we found higher triglyceride concentrations in the livers of TRβ$^-$ and TRβ^{147F} mice but not in TRβ^{GS} mice, replicating the pattern found in serum (Fig. 6 *D* and *F*). The increased serum and hepatic triglyceride concentrations and hepatic triglyceride synthesis in TRβ$^-$ and TRβ^{147F} mice and the similarity of the phenotype in TRβ^{GS} mice to that of WT mice demonstrates that the hypertriglyceridemia is due to the absence of noncanonical TRβ signaling in TRβ$^-$ and TRβ^{147F} mice.

Noncanonical TRβ Signaling Contributes to Regulation of Body Temperature, Oxygen Consumption, and Locomotor Activity. Body temperature homeostasis is crucially linked to TH, and deletion of either TRα or TRβ results in reduced body temperature, although not always significantly (24). By contrast, the mean body temperature of TRβ^{GS} mice was 0.9 °C higher than that of TRβ$^-$ mice and 0.5 °C higher than in WT mice (Fig. 7*A*), suggesting a noncanonical TRβ effect on body temperature. To support this conclusion further, we repeated body temperature measurements in TRβ WT, TRβ$^-$, and TRβ^{GS} mice on a TRα^0 genetic background. Body temperature in TRα^{0}β$^-$ double-KO mice was markedly reduced compared with WT mice (to 34.9 °C vs. 37.0 °C) (Fig. 7*A*), in line with previous reports (24–26). However, the body temperature of TRβ^{GS} mice on the TRα^0 background was ∼1 °C higher than in TRα^{0}β$^-$ double-KO mice (Fig. 7*A*). These results demonstrate a TRβ-specific effect on energy metabolism that is independent of TRα and is mediated via noncanonical actions. We then determined VO_2 by indirect calorimetry and compared the groups using linear regression models including body mass as a covariate. Average VO_2 was increased in TRβ^{GS} mice and reduced in TRβ$^-$ mice compared with WT controls (Fig. 7 *C* and *D* and Table S3). Minimum VO_2 as a proxy of resting metabolic rate was also increased in TRβ^{GS} mice. Food consumption did not differ between genotypes in this short period (Table S3). Furthermore, distance traveled was increased in TRβ^{GS} mice (Fig. 7*B*). Thus, the noncanonical TRβ-specific effects of TH increase the metabolic rate and locomotor activity.

Noncanonical TRα Signaling Contributes to Extrinsic Regulation of Heart Rate. TRα is the predominant TR isoform in the heart, and regulation of heart rate is a well-known physiological effect of TH and TRα (26). We determined heart rate using a noninvasive ECG in untreated WT, TRα^0, and TRα^{GS} mice. Heart rate was significantly reduced in TRα^0 mice compared with WT mice but not in TRα^{GS} mice (Fig. 8*A*). The heart rate in TRα^{GS} mice was normal despite similar reductions in TH target genes known to be involved in heart rate regulation in both TRα^0 and TRα^{GS} mice (Fig. 8*B*). The similar phenotype in WT and TRα^{GS} mice demonstrates that noncanonical TRα signaling contributes to normal heart rate in TRα^{GS} mice. To distinguish between intrinsic and extrinsic cardiac effects, we determined basal heart rate in isolated perfused hearts using a Langendorff apparatus. Ex vivo, the cardiac rhythm was similar in TRα^{GS} and TRα^0 mice (Fig. 8*C*), indicating that noncanonical TRα signaling controls heart rate by an extrinsic mechanism, likely via central regulation of the autonomous nervous system.

Discussion

The physiological role of TRs has been studied in vivo for more than 15 y by comparing WT with TR-KO mice. As both canonical and noncanonical, or type 1 and type 3 (1), TR signaling are present in WT mice, but both are absent in TR-KO mice, such a comparison could not distinguish between the two mechanisms.

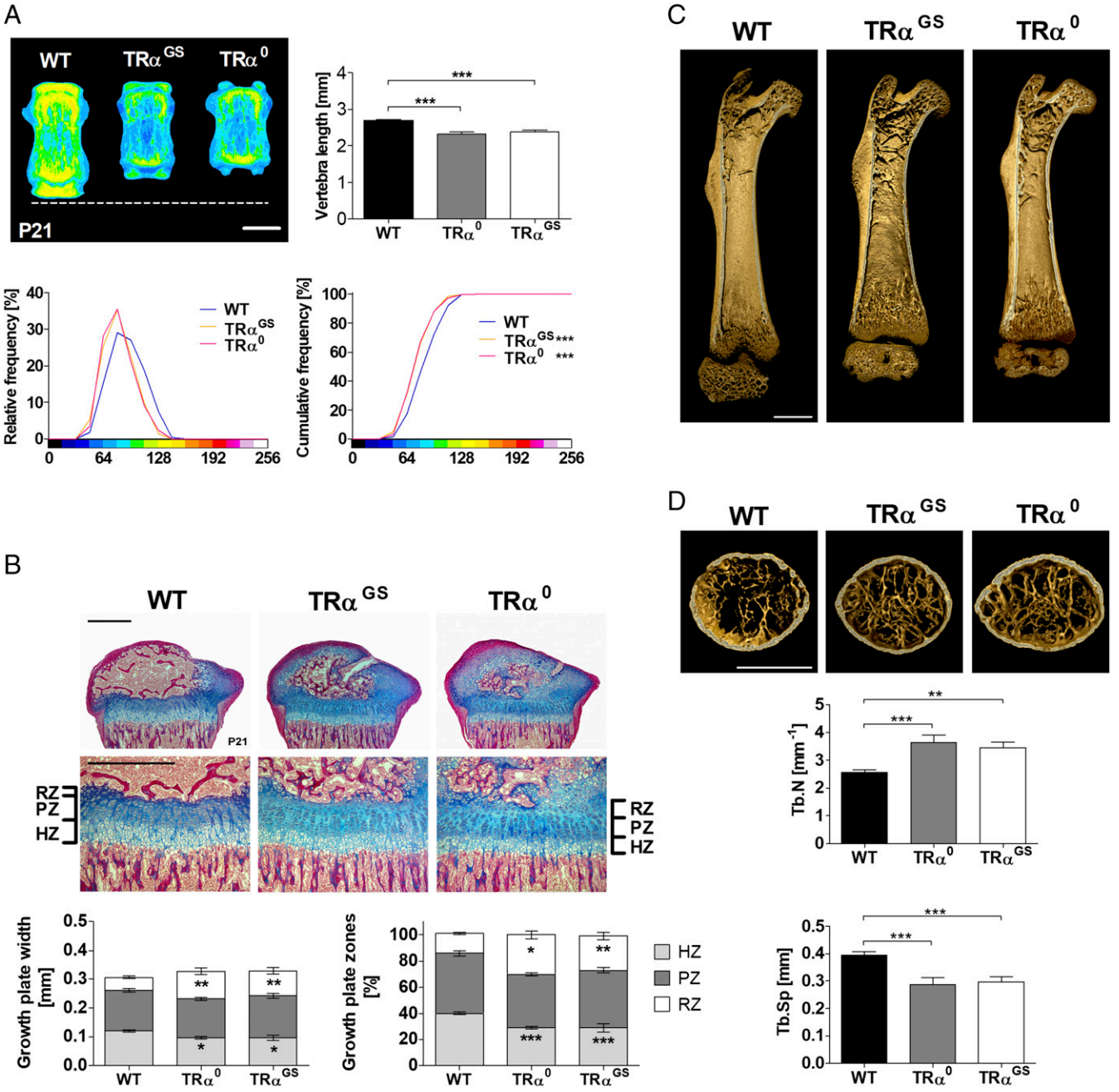

Fig. 5. Canonical TRα action is necessary for normal skeletal development of mice at P21. (*A*, *Upper Left*) Gray-scale images of caudal vertebrae from P21 WT ($n = 8$), TRα^{GS} ($n = 5$), and TRα^{0} ($n = 3$) mice were pseudocolored according to a 16-color palette in which low mineral content is blue and high mineral content is red. (Scale bar, 1,000 μm.) (*Upper Right*) The graph demonstrates caudal vertebra length in WT, TRα^{GS}, and TRα^{0} mice. Data are shown as mean ± SEM; ANOVA and Tukey's post hoc test; ***$P < 0.001$. (*Lower*) Relative (*Left*) and cumulative (*Right*) frequency histograms display bone mineral content of vertebrae from TRα^{GS} and TRα^{0} mice vs. WT mice; Kolmogorov–Smirnov test, ***$P < 0.001$. (*B*, *Upper*) Proximal tibia growth plate sections stained with Alcian blue (cartilage) and van Gieson (bone) (magnification: 50× and 100×, respectively). HZ, hypertrophic zone; PZ, proliferative zone; RZ, reserve zone. (Scale bars, 500 μm.) (*Lower*) Growth plate chondrocyte zone measurements (*Left*) and relative proportions corrected for total growth plate height (*Right*) are shown for WT ($n = 8$), TRα^{GS} ($n = 6$), and TRα^{0} samples; $n = 6$. Data are shown as mean ± SEM; ANOVA and Tukey's post hoc test; *$P < 0.05$; **$P < 0.01$; ***$P < 0.001$. (*C*) Micro-CT images of longitudinal femur midline sections demonstrate bone morphology. (Scale bar: 1,000 μm.) (*D*, *Upper*) Micro-CT images showing transverse sections of the distal metaphysis. (Scale bar: 1,000 μm.) (*Lower*) Graphs demonstrate trabecular number (Tb.N) (*Upper*) and trabecular spacing (Tb.Sp.) (*Lower*). Data are shown as mean ± SEM; ANOVA and Tukey's post hoc test; **$P < 0.01$; ***$P < 0.001$.

To separate both modes of TH/TR signaling, we abolished DNA binding of TRs in TRα^{GS} and TRβ^{GS} mice. Strikingly, despite complete loss of canonical TR signaling, the TRα^{GS} and TRβ^{GS} mice did not exhibit a TR-KO phenotype. Rather, for several established TH effects their phenotype was indistinguishable from WT mice. Thus, these results provide in vivo evidence for the physiological importance of noncanonical TR signaling. Furthermore, they demonstrate that noncanonical TR signaling can be mediated by both TRα and TRβ in an isoform- and tissue-specific manner. These findings have profound implications for the role of TRs in metabolism and physiology and explain the pathophysiology in diseases caused by the various TR mutations.

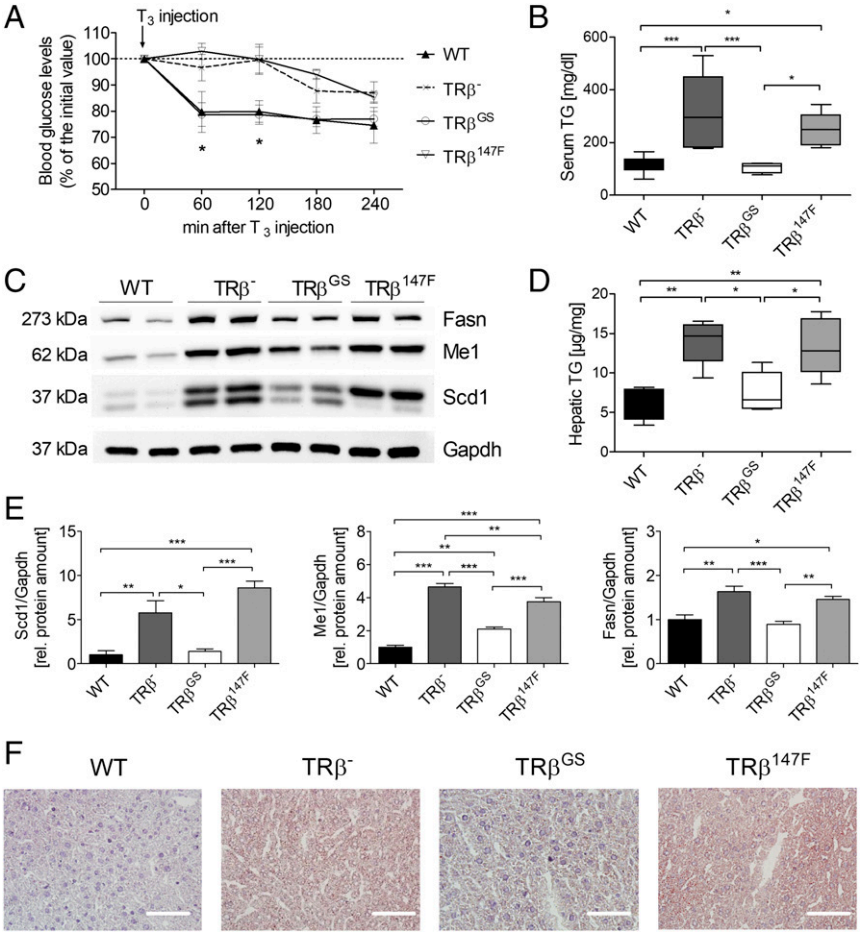

Fig. 6. Noncanonical TRβ signaling influences blood glucose and hepatic triglyceride synthesis. (*A*) Under fasting conditions, WT (black triangles), $TR\beta^{GS}$ (open circles), $TR\beta^{-}$ (**x**), and $TR\beta^{147F}$ (open triangles) mice received a single injection of T_3 (7 ng/g BW), and blood glucose concentration was measured at indicated time points; $n = 4$. Data are shown as mean ± SEM; Student's *t* test; $^{*}P < 0.05$). (*B*) Serum triglyceride concentration in untreated WT (black bar), $TR\beta^{-}$ (dark gray bar), $TR\beta^{GS}$ (open bar), and $TR\beta^{147F}$ (light gray bar) mice. (*C*) Representative immunoblots against *Fasn*, *Me1*, and *Scd1* from liver samples. *Gapdh* was used as loading control; $n = 2$. (*D*) Triglyceride concentration in liver tissue was assessed after lipid extraction; $n = 4$–6 mice per genotype. Horizontal bars in the box plots indicate mean values, and whiskers indicate minimum and maximum values; ANOVA and Bonferroni's post hoc test for multiple comparison; $^{*}P < 0.05$; $^{**}P < 0.01$; $^{***}P < 0.001$. (*E*) Immunoblots against Scd1 (*Left*), Me1 (*Center*), and Fasn *Right*), with a group size of $n = 4$ were used for densitometric measurements. Data are shown as mean ± SEM; ANOVA with Tukey's post hoc test; $^{*}P < 0.05$; $^{**}P < 0.01$; $^{***}P < 0.001$. (*F*) Oil red O staining of liver sections from untreated WT, $TR\beta^{-}$, $TR\beta^{GS}$, and $TR\beta^{147F}$ mice was done to visualize triglycerides in liver tissue. (Scale bar: 50 µm.)

Canonical Actions of TRs. An important physiological role of TH is negative feedback in the HPT axis. $TR\beta^{GS}$ mice had a phenotype similar to that of $TR\beta^{-}$ mice with lack of TRβ-mediated negative feedback in the pituitary and TH resistance (9), whereas the HPT axis in $TR\beta^{147F}$ mice was unaffected (7). A higher TSH in $TR\beta^{GS}$ mice could indicate that they are slightly more resistant than the $TR\beta^{-}$ mice. A potential but highly speculative explanation is cofactor squelching. TRβGS does not bind to DNA but is still capable of cofactor binding. This could, theoretically, reduce cofactor availability for TRα and reduce a minimal repressive TRα effect on TSH expression, resulting in even higher TSH concentrations than in TRβ-KO mice. Delayed longitudinal growth and bone mineralization are typical features of $TR\alpha^{0}$ mice and were replicated in $TR\alpha^{GS}$ mice. Therefore negative regulation of the HPT axis in $TR\beta^{GS}$ mice and bone development in $TR\alpha^{GS}$ mice are solely dependent on canonical TR/TRE-mediated transcriptional regulation. Nevertheless, a recently identified short variant of TRα, p30 TRα1, associates with the plasma membrane, increases nitric oxide and cGMP production, and activates the ERK and PI3K pathways in vitro (27). Furthermore, it has been suggested that p30 TRα may have a role in the regulation of adult bone formation. Here, we studied bone development in 3-wk-old mice and determined linear growth until cessation of the experiment at 10 wk of age. While skeletal development and linear growth were unequivocally canonical, we cannot exclude a contribution of noncanonical actions of TRα in adult bone remodeling.

Noncanonical Actions of TRβ. Serum glucose decreased rapidly only in WT and $TR\beta^{GS}$ mice but not in $TR\beta^{-}$ and $TR\beta^{147F}$ mice despite intact canonical TRβ signaling in the $TR\beta^{147F}$ mice. The phenotype in $TR\beta^{GS}$ mice demonstrates that noncanonical TRβ action alone suffices to generate physiological responses. Similarly, triglyceride synthesis and serum and liver triglyceride content were elevated in $TR\beta^{-}$ and $TR\beta^{147F}$ mice that lack noncanonical TRβ action, suggesting reduced consumption of triglyceride substrates. Body temperature was higher in $TR\beta^{GS}$ than in WT mice, probably as a consequence of elevated serum TH concentration due to the disruption of the HPT axis in these mice and the retained noncanonical action of $TR\beta^{GS}$. Additionally, VO_2 and distance traveled were higher in $TR\beta^{GS}$ mice. Increased energy metabolism, body temperature, and locomotor activity and lower triglyceride concentrations are physiological consequences of noncanonical TRβ action.

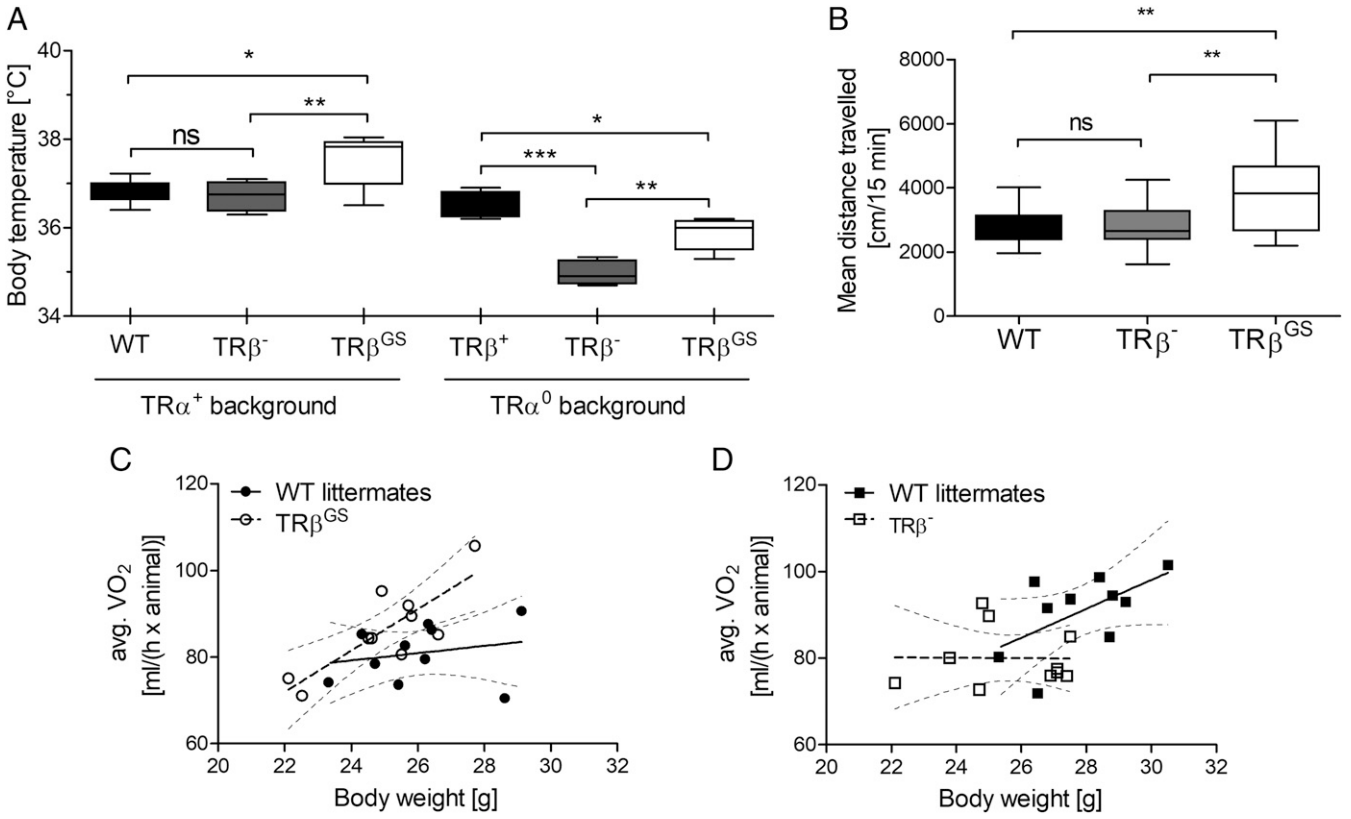

Fig. 7. Noncanonical action of TRβ increases body temperature, VO_2, and locomotor activity. (*A*) Body temperature of male mice in a $TR\alpha^+$ (WT) or a $TR\alpha^0$ genetic background; $n = 6$. Box plots indicate mean values, and whiskers indicate minimum and maximum values; ANOVA and Bonferroni's post hoc test for multiple comparison; ns, not significant; $^*P < 0.05$; $^{**}P < 0.01$; $^{***}P < 0.001$. (*B*) Locomotor activity of WT, $TR\beta^-$, and $TR\beta^{GS}$ mice expressed as centimeters traveled in 15 min; $n = 10$–20 mice per genotype. Horizontal bars in the box plots indicate mean values, and whiskers indicate minimum and maximum values; ANOVA with Tukey's post hoc test; $^{**}P < 0.01$, ns, not significant. (*C* and *D*) Average VO_2 of $TR\beta^{GS}$ (*C*) and $TR\beta^-$ mice (*D*) and WT littermate controls was measured by indirect calorimetry and is plotted against body weight ($n = 10$).

Noncanonical Actions of TRα. Noncanonical TH effects on the cardiovascular system have been reported, especially a rapid decrease in blood pressure and PI3K signaling pathway activation in the heart (28–30). In $TR\alpha^{GS}$ mice the heart rate in vivo was similar to that in WT mice, but, consistent with the expression of cardiac pacemaker genes, the ex vivo cardiac rate in $TR\alpha^{GS}$ hearts was similar to that of $TR\alpha^0$ hearts. These results suggest that the noncanonical TH/TRα mechanism contributing to normal heart rate in vivo is not intrinsic to the heart. As ECG data were obtained from mice without anesthesia, it is possible that the response to stress or the activity of the sympathetic nervous system was reduced in $TR\alpha^0$ mice but preserved in $TR\alpha^{GS}$ mice. Therefore we propose that noncanonical TH/TRα action influences heart rate via the autonomous nervous system and not via direct actions in the heart. Interestingly, this appears to be similar to the regulation of locomotor activity, which also is likely centrally mediated. Where and how TRα acts has yet to be determined.

Evolution of Noncanonical TH Signaling. Our findings suggest that increased noncanonical TRβ signaling increases energy metabolism and body temperature. Support for this interpretation may be derived from evolution: TH stimulates thermogenesis in homeothermy, a feature of mammals. Interestingly, the tyrosine motifs in TRβ, which are required for noncanonical PI3K activation by TRβ, are found in all mammalian TRβ ortholog sequences but not in sequences from poikilothermic animals, such as alligator, clawed toad, or zebrafish (7). Hence, noncanonical TR signaling may be a recently acquired adaptation in evolution that provides mammals with a novel mechanism by which TH can regulate energy metabolism, body temperature, and activity. Development of noncanonical TR signaling relatively late in evolution, long after TRs assumed their canonical role as ligand-dependent transcription factors, may also explain why the physiological effects of canonical and noncanonical TR signaling are so clearly distinct from one another.

Negative Regulation of Gene Expression. A persisting point of controversy is whether DNA binding of TRs is required for negative regulation of gene expression by TRs. TSH elevation in $TR\beta^-$ and $TR\beta^{GS}$ mice clearly demonstrates that, in agreement with previous reports (9), inhibition of TSH expression in vivo requires DNA binding. Results from $TR\beta^{GS}$ mice indicate that noncanonical TH action may contribute to negative regulation. *Scd1* expression in HepG2 cells and in mouse liver is negatively regulated by TH (Fig. S5) (31). Compared with WT mice, hepatic *Scd1* expression was elevated in $TR\beta^-$ mice but not in $TR\beta^{GS}$ mice. Therefore, negative regulation of *Scd1* expression in vivo does not require DNA binding of TRβ. In microarray studies, however, we did not detect down-regulation of *Scd1* within 6 h. Two explanations seem plausible: Either *Scd1* is directly negatively regulated by TH/TRβ without DNA binding by an unknown mechanism that takes longer than 6 h or down-regulation of *Scd1* in liver is only a secondary effect in response to noncanonical TRβ effects on metabolism, which also take more than 6 h. The fact that, in addition to *Scd1*, several other genes involved in triglyceride synthesis also were negatively regulated by T_3 suggests the latter. Repression of these genes appears to be a coordinated response to reduced substrate availability for triglyceride synthesis, possibly due to increased metabolism. Repression of *Myh7* appeared to be partially preserved in hearts of

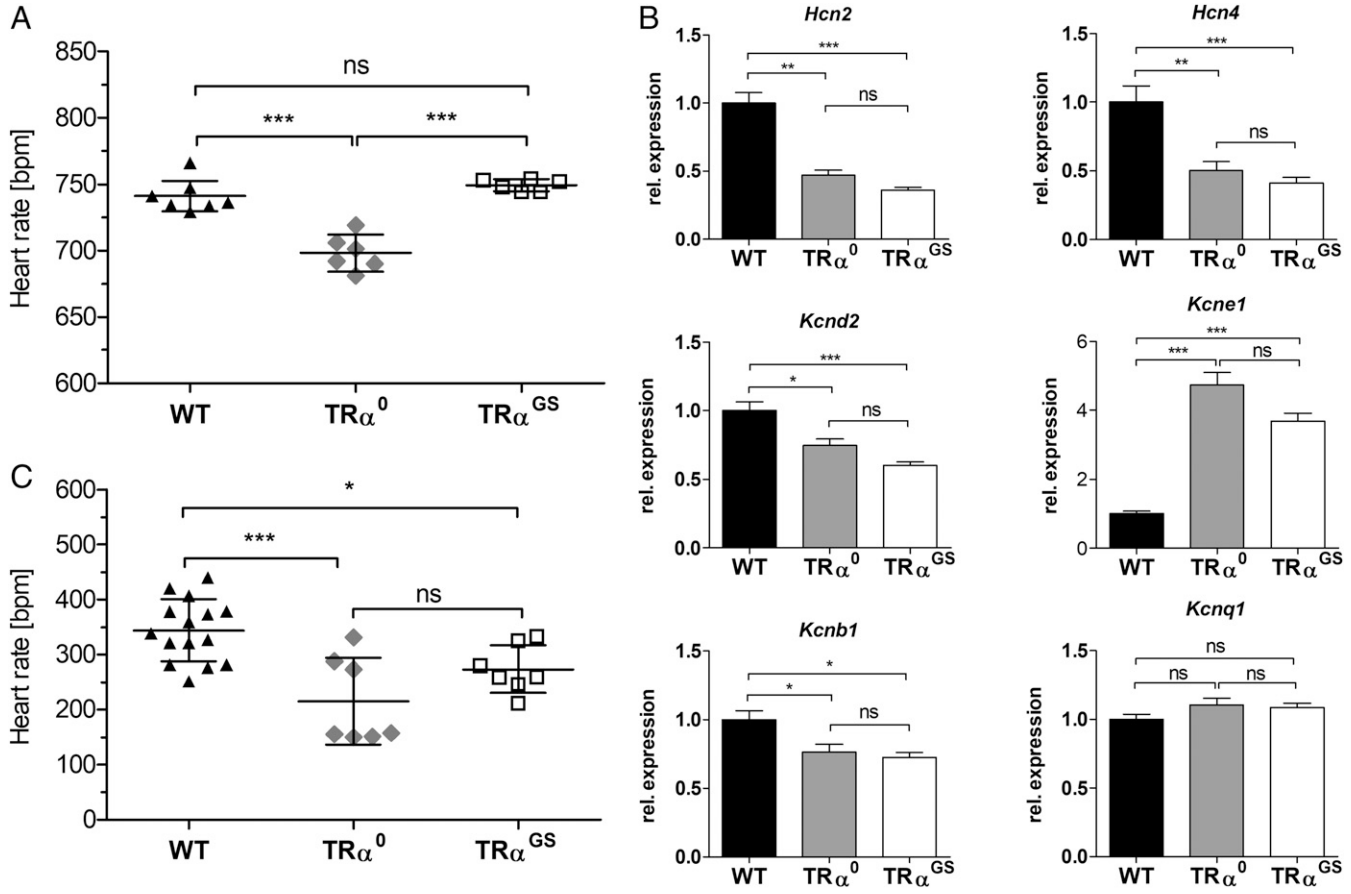

Fig. 8. Noncanonical TRα signaling maintains normal basal heart rate without altering cardiac pacemaker channel gene expression. (*A*) Heart rate of nonsedated male WT (black triangles; $n = 7$), $TR\alpha^0$ (gray diamonds; $n = 6$), and $TR\alpha^{GS}$ (open squares; $n = 6$) mice. Data are shown as mean ± SD; ANOVA followed by Bonferroni's post hoc test for multiple comparisons; $***P < 0.0001$; ns, not significant. (*B*) Relative expression of pacemaker channels *Hcn2* and *Hcn4* and of potassium channel subunits with importance for repolarization (*Kcnd2*, *Kcne1*, *Kcnb1*, and *Kcnq1*) in hearts of WT (black bars),$TR\alpha^0$ (gray bars), and $TR\alpha^{GS}$ (open bars) mice; $n = 6$. Data are shown as mean ± SEM; ANOVA and Tukey's post hoc test; $*P < 0.05$; $**P < 0.01$; $***P < 0.001$; ns, not significant. (*C*) Ex vivo heart rate measured in hearts isolated from untreated WT (black triangles; $n = 15$), $TR\alpha^0$ (gray diamonds; $n = 8$), or $TR\alpha^{GS}$ (open squares; $n = 7$) mice. Data are shown as mean ± SD; ANOVA followed by Tukey's post hoc test; $*P < 0.05$; $***P < 0.0001$; ns, not significant.

$TR\alpha^{GS}$ mice. Expression of *Myh7* is negatively regulated by miRNA miR-208a, which is encoded by an intronic sequence of *Myh6*. Repression of *Myh7* by increased TH concentration is an indirect effect of *Myh6* induction and, consequently, miR-208a expression. Our interpretation of the difference in *Myh7* expression in $TR\alpha^0$ and $TR\alpha^{GS}$ mice is that the relationship between *Myh6* and *Myh7* may not be linear. However, a partial noncanonical repressive effect of TRαGS cannot be ruled out.

Role of Noncanonical PI3K Activation. The best-studied noncanonical action of TRβ is rapid activation of PI3K (5–7). We therefore studied the $TR\beta^{147F}$ mouse as a control, because in this mouse model the activation of PI3K by TRβ is selectively abrogated. In the blood glucose response to T_3 and serum and liver triglyceride concentrations, the phenotype of $TR\beta^{147F}$ mice was similar to that of $TR\beta^-$ mice, demonstrating that these effects are indeed mediated by TRβ activation of PI3K. As insulin also signals via PI3K to decrease blood glucose by increasing the translocation of glucose transporter 4 (GLUT4) to the plasma membrane, we hypothesize that insulin and noncanonical TRβ signaling converge at the PI3K pathway. This mechanism of TRβ action would explain previous observations in which T_3 treatment increased glucose uptake into the thymus in rats independent of protein synthesis (32), increased glucose uptake into L6 muscle cells in a PI3K-depentent manner in vitro (33), and increased the translocation of GLUT4 in skeletal muscle of rats (34). TRα also activates signaling pathways (29, 35), possibly as a short p30 TRα variant that indirectly activates ERK and PI3K after T_3 binding and nitric oxide and cGMP production (27) or by direct protein–protein interaction between TRα and PI3K (29, 35, 36). The noncanonical mechanism by which TRα influences heart rate remains unknown.

In conclusion, noncanonical, DNA-independent TR signaling contributes significantly to the physiological actions of TH, and these noncanonical actions appear to predominantly regulate energy homeostasis. These findings demonstrate that TRα and TRβ mediate both canonical and noncanonical signaling in vivo, establishing a paradigm shift for TH action.

Materials and Methods

Extended and detailed material and methods are provided in *Supporting Information*. All animal studies were approved by the local authorities (Landesamt für Natur, Umwelt und Verbraucherschutz Nordrhein-Westfalen). All tests performed at the German Mouse Center (GMC) were approved by the responsible authority of the Regierung von Oberbayern. TRα and TRβ WT and KO and $TR\beta^{147F}$ mice were genotyped as previously described (7, 24, 37). $TR\beta^{147F}$ mice were provided by D.L.A. (7). TR-GS mice were generated via the zinc finger nuclease approach (CompoZr Targeted Integration-Kit-AAVS; Sigma-Aldrich) (38, 39). Mice were rendered hypothyroid by maintenance on a low-iodine diet and administration of methimazole and perchloride via the drinking water. Animals were treated with experiment-specific concentrations of T_3 by i.p. injections. Serum TSH was measured as previously described (40), and TH serum concentrations were determined by ELISA (DRG Diagnostics). Bone morphology

and histology were investigated with standardized methods described in detail in *Supporting Information* and refs. 18 and 19. Body temperature was determined with a rectal probe, and blood glucose was measured with a Contour XT glucometer (Bayer). Indirect calorimetry was performed at the GMC (Munich) according to standardized in-house protocols. Heart rate was determined either with an ECG in fully conscious mice or ex vivo via Langendorff apparatus. Experimental procedures for transfection, luciferase reporter assay, fluorescent EMSA, qRT-PCR (41), Oil red O staining, and immunoblotting have been published previously and are described together with fluorescent DNA probes, primers, and antibodies in *Supporting Information*. Microarray was done with a MG-430_2.0 gene chip (Affymetrix). ChIP and ChIP-seq were performed as previously described (12, 42) with minor modifications explained in *Supporting Information*. Microarray and ChIP-seq data have been deposited in the National Center for Biotechnology Information (NCBI) Gene Expression Omnibus (GEO) database (43) and are accessible through the following GEO Series accession numbers: GSE93864 (microarray) and GSE104877 (ChIP-seq). Statistical analysis was performed with GraphPad Prism6, and differences were considered significant when $P < 0.05$.

ACKNOWLEDGMENTS. We thank B. Gloss at the National Institute of Environmental Health Sciences for providing breeding pairs of TRβ^{147F} mice. Illumina sequencing was performed by Ronni Nielsen with support from the VILLUM Center for Bioanalytical Sciences at the University of Southern Denmark. The TR C1 antibody was provided by Sheue-yann Cheng of the NIH. This work was supported by Deutsche Forschungsgemeinschaft Grants MO1018/2-1/2 (to L.C.M.), FU356/7-1 (to D.F.), and KO 922/17-1/2 (to J.K.) within the priority program Thyroid Trans Act SPP 1629; by Charité funds (J.K.); and in part by NIH Grant R37DK15070 (to S.R.), the Seymour J. Abrams Fund for Thyroid Research, Wellcome Trust Strategic Award 101123, and Wellcome Trust Project Grant 094134 (to J.H.D.B. and G.R.W.). Studies at the GMC were supported by German Federal Ministry of Education and Research Infrafrontier Grant 01KX1012 (to M.H.d.A.). L.G. was supported by grants from the Lundbeck Foundation and Novo Nordisk Foundation. D.L.A. was supported by Award Z01-ES102285 from the Intramural Program at the National Institute of Environmental Health Sciences of the NIH. The content is solely the responsibility of the authors and does not necessarily represent the official views of the National Institute of Diabetes and Digestive and Kidney Diseases or the NIH.

1. Flamant F, et al. (2017) Thyroid hormone signaling pathways. Time for a more precise nomenclature. *Endocrinology* 158:2052–2057.
2. Yen PM (2001) Physiological and molecular basis of thyroid hormone action. *Physiol Rev* 81:1097–1142.
3. Ortiga-Carvalho TM, Sidhaye AR, Wondisford FE (2014) Thyroid hormone receptors and resistance to thyroid hormone disorders. *Nat Rev Endocrinol* 10:582–591.
4. Storey NM, O'Bryan JP, Armstrong DL (2002) Rac and Rho mediate opposing hormonal regulation of the ether-a-go-go-related potassium channel. *Curr Biol* 12:27–33.
5. Cao X, Kambe F, Moeller LC, Refetoff S, Seo H (2005) Thyroid hormone induces rapid activation of Akt/protein kinase B-mammalian target of rapamycin-p70S6K cascade through phosphatidylinositol 3-kinase in human fibroblasts. *Mol Endocrinol* 19:102–112.
6. Storey NM, et al. (2006) Rapid signaling at the plasma membrane by a nuclear receptor for thyroid hormone. *Proc Natl Acad Sci USA* 103:5197–5201.
7. Martin NP, et al. (2014) A rapid cytoplasmic mechanism for PI3 kinase regulation by the nuclear thyroid hormone receptor, TRβ, and genetic evidence for its role in the maturation of mouse hippocampal synapses in vivo. *Endocrinology* 155:3713–3724.
8. Shibusawa N, Hollenberg AN, Wondisford FE (2003) Thyroid hormone receptor DNA binding is required for both positive and negative gene regulation. *J Biol Chem* 278: 732–738.
9. Shibusawa N, et al. (2003) Thyroid hormone action in the absence of thyroid hormone receptor DNA-binding in vivo. *J Clin Invest* 112:588–597.
10. Ayers S, et al. (2014) Genome-wide binding patterns of thyroid hormone receptor beta. *PLoS One* 9:e81186.
11. Ramadoss P, et al. (2014) Novel mechanism of positive versus negative regulation by thyroid hormone receptor β1 (TRβ1) identified by genome-wide profiling of binding sites in mouse liver. *J Biol Chem* 289:1313–1328.
12. Grøntved L, et al. (2015) Transcriptional activation by the thyroid hormone receptor through ligand-dependent receptor recruitment and chromatin remodelling. *Nat Commun* 6:7048.
13. Sakurai A, et al. (1989) Generalized resistance to thyroid hormone associated with a mutation in the ligand-binding domain of the human thyroid hormone receptor beta. *Proc Natl Acad Sci USA* 86:8977–8981.
14. Forrest D, et al. (1996) Recessive resistance to thyroid hormone in mice lacking thyroid hormone receptor beta: Evidence for tissue-specific modulation of receptor function. *EMBO J* 15:3006–3015.
15. Weiss RE, et al. (1997) Thyrotropin regulation by thyroid hormone in thyroid hormone receptor beta-deficient mice. *Endocrinology* 138:3624–3629.
16. Abel ED, Ahima RS, Boers ME, Elmquist JK, Wondisford FE (2001) Critical role for thyroid hormone receptor beta2 in the regulation of paraventricular thyrotropin-releasing hormone neurons. *J Clin Invest* 107:1017–1023.
17. Bassett JH, Williams GR (2016) Role of thyroid hormones in skeletal development and bone maintenance. *Endocr Rev* 37:135–187.
18. Bassett JH, et al. (2010) Optimal bone strength and mineralization requires the type 2 iodothyronine deiodinase in osteoblasts. *Proc Natl Acad Sci USA* 107:7604–7609.
19. Bassett JH, et al. (2014) Thyroid hormone receptor α mutation causes a severe and thyroxine-resistant skeletal dysplasia in female mice. *Endocrinology* 155:3699–3712.
20. Lin Y, Sun Z (2011) Thyroid hormone potentiates insulin signaling and attenuates hyperglycemia and insulin resistance in a mouse model of type 2 diabetes. *Br J Pharmacol* 162:597–610.
21. Petersson U, Kjellström T (2001) Thyroid function tests, serum lipids and gender interrelations in a middle-aged population. *Scand J Prim Health Care* 19:183–185.
22. Johansson L, et al. (2005) Selective thyroid receptor modulation by GC-1 reduces serum lipids and stimulates steps of reverse cholesterol transport in euthyroid mice. *Proc Natl Acad Sci USA* 102:10297–10302.
23. Araki O, Ying H, Zhu XG, Willingham MC, Cheng SY (2009) Distinct dysregulation of lipid metabolism by unliganded thyroid hormone receptor isoforms. *Mol Endocrinol* 23:308–315.
24. Gauthier K, et al. (2001) Genetic analysis reveals different functions for the products of the thyroid hormone receptor alpha locus. *Mol Cell Biol* 21:4748–4760.
25. Wikström L, et al. (1998) Abnormal heart rate and body temperature in mice lacking thyroid hormone receptor alpha 1. *EMBO J* 17:455–461.
26. Macchia PE, et al. (2001) Increased sensitivity to thyroid hormone in mice with complete deficiency of thyroid hormone receptor alpha. *Proc Natl Acad Sci USA* 98: 349–354.
27. Kalyanaraman H, et al. (2014) Nongenomic thyroid hormone signaling occurs through a plasma membrane-localized receptor. *Sci Signal* 7:ra48.
28. Schmidt BM, et al. (2002) Nongenomic cardiovascular effects of triiodothyronine in euthyroid male volunteers. *J Clin Endocrinol Metab* 87:1681–1686.
29. Hiroi Y, et al. (2006) Rapid nongenomic actions of thyroid hormone. *Proc Natl Acad Sci USA* 103:14104–14109.
30. Kuzman JA, Vogelsang KA, Thomas TA, Gerdes AM (2005) L-Thyroxine activates Akt signaling in the heart. *J Mol Cell Cardiol* 39:251–258.
31. Hashimoto K, et al. (2013) Human stearoyl-CoA desaturase 1 (SCD-1) gene expression is negatively regulated by thyroid hormone without direct binding of thyroid hormone receptor to the gene promoter. *Endocrinology* 154:537–549.
32. Segal J, Ingbar SH (1985) In vivo stimulation of sugar uptake in rat thymocytes. An extranuclear action of 3,5,3′-triiodothyronine. *J Clin Invest* 76:1575–1580.
33. Gordon A, Swartz H, Shwartz H (2006) 3,5,3′ Triiodo-L-thyronine stimulates 2-deoxy-D-glucose transport into L6 muscle cells through the phosphorylation of insulin receptor beta and the activation of PI-3k. *Thyroid* 16:521–529.
34. Brunetto EL, Teixeira SdaS, Giannocco G, Machado UF, Nunes MT (2012) T3 rapidly increases SLC2A4 gene expression and GLUT4 trafficking to the plasma membrane in skeletal muscle of rat and improves glucose homeostasis. *Thyroid* 22:70–79.
35. Cao X, Kambe F, Yamauchi M, Seo H (2009) Thyroid-hormone-dependent activation of the phosphoinositide 3-kinase/Akt cascade requires Src and enhances neuronal survival. *Biochem J* 424:201–209.
36. Furuya F, et al. (2013) Ligand-bound thyroid hormone receptor contributes to reprogramming of pancreatic acinar cells into insulin-producing cells. *J Biol Chem* 288: 16155–16166.
37. Gauthier K, et al. (1999) Different functions for the thyroid hormone receptors TRalpha and TRbeta in the control of thyroid hormone production and post-natal development. *EMBO J* 18:623–631.
38. Carbery ID, et al. (2010) Targeted genome modification in mice using zinc-finger nucleases. *Genetics* 186:451–459.
39. Cui X, et al. (2011) Targeted integration in rat and mouse embryos with zinc-finger nucleases. *Nat Biotechnol* 29:64–67.
40. Pohlenz J, et al. (1999) Improved radioimmunoassay for measurement of mouse thyrotropin in serum: Strain differences in thyrotropin concentration and thyrotroph sensitivity to thyroid hormone. *Thyroid* 9:1265–1271.
41. Bustin SA, et al. (2009) The MIQE guidelines: Minimum information for publication of quantitative real-time PCR experiments. *Clin Chem* 55:611–622.
42. Siersbæk M, et al. (2017) High fat diet-induced changes of mouse hepatic transcription and enhancer activity can be reversed by subsequent weight loss. *Sci Rep* 7:40220.
43. Edgar R, Domrachev M, Lash AE (2002) Gene expression omnibus: NCBI gene expression and hybridization array data repository. *Nucleic Acids Res* 30:207–210.
44. Samuels HH, Stanley F, Casanova J (1979) Depletion of L-3,5,3′-triiodothyronine and L-thyroxine in euthyroid calf serum for use in cell culture studies of the action of thyroid hormone. *Endocrinology* 105:80–85.
45. Dobin A, et al. (2013) STAR: Ultrafast universal RNA-seq aligner. *Bioinformatics* 29:15–21.
46. Heinz S, et al. (2010) Simple combinations of lineage-determining transcription factors prime cis-regulatory elements required for macrophage and B cell identities. *Mol Cell* 38:576–589.
47. Love MI, Huber W, Anders S (2014) Moderated estimation of fold change and dispersion for RNA-seq data with DESeq2. *Genome Biol* 15:550.
48. Kolde R (2015) Pretty Heatmaps. R Package, Version 1.0.8. Available at https://cran.r-project.org/web/packages/pheatmap/index.html. Accessed August 9, 2017.
49. Pfaffl MW (2001) A new mathematical model for relative quantification in real-time RT-PCR. *Nucleic Acids Res* 29:e45.
50. Hildebrandt HA, et al. (2016) Kinetics and signal activation properties of circulating factor(s) from healthy volunteers undergoing remote ischemic pre-conditioning. *JACC Basic Transl Sci* 1:3–13.

Supporting Information

Hönes et al. 10.1073/pnas.1706801115

SI Materials and Methods

TR Expression Vectors. Point mutations for TRα71GS, TRαG291R, TRβ125GS, TRβG345R, and TRβY147F were introduced into pcDNA3 vectors expressing TRα1 and TRβ1 by site-directed mutagenesis (QuikChange Site Directed Mutagenesis Kit; Agilent Technologies). Please see Dataset S1 for primer sequences.

Cell Culture and Transfection. HEK293 cells, obtained from ATCC, were used for in vitro experiments. Cells were maintained in DMEM containing 4.5 g/L glucose, pyruvate (DMEM + GlutaMAX; Gibco), 1% ZellShield (Minerva Biolabs GmbH), and 10% FCS (Gibco). For transient transfection, 4×10^4 HEK293 cells were grown to 80% confluence in 24-well plates. FuGENE6 (Promega) transfection reagent was used in a 1:3 DNA:FuGENE ratio.

EMSA. TRα, TRα71GS, TRβ, TRβ125GS, TRβY147F, and RXRα proteins were generated using a reticulocyte transcription and translation kit (TNT T7; Promega) and 1 μg of the respective plasmid. Four microliters of translated TR and 2 μL of RXRα were preincubated in reaction buffer (10 mM Tris, 50 mM KCl, 1 mM DTT, and 5% glycerol with 1 μg of poly-dI:dC) for 10 min at 20 °C before 1 μL of 5′-Cy5–labeled DR4 probe (Cy5 5′-GCTATGAGGTCACAGGAGGTCATGCAAC-3′) was added to achieve a final concentration of 1 pmol/μL. After 30 min incubation at 20 °C the protein–DNA complexes were analyzed on a 6% polyacrylamide gel (0.5× Tris-borate-EDTA, 89 mM Tris-base, 89 mM borate, 2 mM EDTA). The fluorescent probe was visualized using a VersaDoc imaging system (Bio-Rad).

Luciferase Assay. HEK293 cells were transiently transfected using 280 ng per well of DR-4-TKLuc-reporter plasmid, 33 ng per well RL-TK control plasmid, and 17 ng per well of plasmid encoding for TRα1 or TRβ1 variants (TRα, TRα71GS, TRαG291R, TRβ, TRβ125GS, TRβG345R, TRβY147F, or empty vector pcDNA3) in the absence of FCS. After 24 h, the transfection medium was replaced by fresh medium containing 5% TH-depleted FCS, which was generated by treatment with anion-exchange resin as previously described (44). Cells were stimulated with 10 nM T_3 (dissolved in 40 mM NaOH, 0.002% BSA) or were treated with vehicle for another 48 h. Cells were harvested, and the activities of firefly and renilla luciferases were determined (Dual-Glo Luciferase Assay System; Promega) in a Sirius luminometer (Berthold Detection Systems GmbH). Firefly luciferase luminescence was normalized to renilla luciferase luminescence from the same transfection sample to control for transfection efficiency.

Generation of TRα^{GS} and TRβ^{GS} Knockin Mice. The GS point mutations were introduced into the *Thra* (NM_178060.3) and *Thrb* (NM_001113417.1) gene loci of C57BL/6J mice using custom-made zinc finger nucleases (ZFNs) (CompoZr Targeted Integration Kit-AAVS; Sigma-Aldrich) and a donor plasmid containing the desired sequence (38, 39). For *Thra* we chose a ZFN cutting site within exon 3, 42 bp upstream from the target codons, and for *Thrb* the ZFN cutting site was chosen downstream of exon 3 (ZNF recognition sequence for *Thra*: 5′-TCC CTA GTT ACC TGGA *CAAAGAC* ACG AGC AGT GTG TCG TGT GTG-3′; for *Thrb*: 5′-CCA GAC AAC CAC *TGGACAT* CAGG CTT ACA GAA AGA GAT-3′; the ZFN binding sites are underlined, and the *FokI* cutting sites are in italics). The donor vectors pTRαGS-donor and pTRβGS-donor (both in pUC57-Kan; GENEWIZ) contained the mutations changing the amino acid sequence in the TR P-box from glutamic acid (E) and glycine (G) to glycine and serine (S). The codons 71, GAG, and 72, GGC, of exon 3 of *Thra* were mutated to GGG and AGC, respectively. Corresponding codons in *Thrb* (125, GAA, and 126, GGC) were changed to GGA and AGC, respectively. Additionally, silent mutations created artificial restriction sites for EcoRV (TRα^{GS}) and Mph1103I (TRβ^{GS}) to facilitate genotyping by restriction-fragment length polymorphism (RFLP)-PCR (Fig. S6). C57BL/6JCrl oocytes were injected with microinjection solution (MIS) containing 20 ng/μL ZFN mRNA and 1.3 ng/μL donor plasmid. Injection of 1 pL MIS per pronucleus was performed with Leica micromanipulators. Manipulated oocytes were transplanted into oviducts of 0.5-d postconception pseudopregnant mice. Offspring were screened by PCR and sequencing, which confirmed the successful TRα$^{GS/+}$ and TRβ$^{GS/+}$ knockin mutations. One pup out of 29 for TRα$^{GS/+}$ and one out of 39 for TRβ$^{GS/+}$ was positive for the targeted integration, representing mutation rates of 3.5% and 2.6%, respectively. Homozygous TRα^{GS} and TRβ^{GS} mice were born in Mendelian proportions. These mice were viable, and no effect on fertility was observed in breeding animals up to the age of 8 mo. Genotyping of TRβ^{GS} mice was performed by RFLP using the forward primer mTRβ-fwd (5′-TCT GAA GCA CCA ACA CTT TCC T-3′) located on the genomic *Thrb* sequence upstream of the 3′-homology region of the donor vector and the reverse primer mTRβ-rev (5′-AGA AAG GCT GTG GAG CAA AC-3′) binding downstream of exon 3, generating a 1,399-bp amplicon. For TRα^{GS} we used mTRα-fwd (5′-GTT TTG GCC CCA TCT AAG CC-3′) and mTRα-rev (5′-AGC CGT GCC AGG TGA ATT AG-3′). Digestion of the PCR product with EcoRV (TRα$^{GS/+}$) or Mph1103I (TRβ$^{GS/+}$) indicated the GS allele (both enzymes were purchased from Thermo Fisher Scientific). TR-KO (TRα^0 and TRβ$^-$) mice were obtained from the European Mouse Mutant Archive (https://www.infrafrontier.eu). TRβ^{147F} mice were provided by D.L.A. (7). TRα and TRβ WT and KO and TRβ^{147F} mice were genotyped as previously described (7, 24, 37). All mouse strains were kept on a C57BL/6JCrl backcross for at least five generations. All experiments were performed with homozygotes.

Animal Treatment and Phenotyping. Animal studies were approved by the local authorities (Landesamt für Natur, Umwelt und Verbraucherschutz Nordrhein-Westfalen). Mice were housed at 21 ± 1 °C on an alternating 12-h light/12-h dark cycle. Standard chow (Ssniff) and tap water were provided ad libitum, unless indicated otherwise. All tests performed at the GMC were approved by the responsible authority of the Regierung von Oberbayern. Mice were maintained in individually ventilated cages with water and standard mouse chow according to the GMC housing conditions and German laws. After 15 wk WT, TRα^0, TRα^{GS}, TRβ$^-$, and TRβ^{GS} animals were killed to obtain serum and tissue samples. Tail length and BW were recorded for all genotypes from P21 through week 10. Bone samples were taken from WT, TRα^0, and TRα^{GS} mice at P21. The body temperature of 12- to 13-wk-old male WT, TRβ$^-$, and TRβ^{GS} mice was measured every other day between 9 and 10 AM with a rectal probe (TempJKT; Eutech Instruments). Heart rate was determined in WT, TRα^0, and TRα^{GS} mice without anesthesia using noninvasive ECG and at least three recordings per mouse. ECG data were analyzed with PicoScope 6 (Pico Technology). For in vivo studies of T_3 effects on gene expression, WT, TRβ$^-$, TRβ^{GS}, and TRβ^{147F} mice were rendered hypothyroid at the age of 10–11 wk with an iodine-deficient diet (TD.95007; Harlan-Teklad) with 0.05% 2-mercapto-1-methylimidazole (MMI), and

1% potassium perchlorate (Sigma-Aldrich) administered in the drinking water. After 3 wk, mice were separated into T_3-treatment and control groups for each genotype. T_3-treated animals received T_3 (Sigma-Aldrich), 200 ng/g BW, i.p. once as a single dose (for microarray, ChIP, and ChIP-seq analyses) or daily for 5 d (for real-time PCR). Animals in the control group were injected with vehicle i.p. The mice were killed with CO_2 6 h after the single dose of T_3 or 2 h after the last injection on day 5, and blood and tissue samples were collected. To measure the blood glucose response to T_3, WT, TRβ$^-$, TRβ^{GS}, and TRβ^{147F} mice were injected i.p. with T_3 (7 ng/g BW) or vehicle. Blood was drawn by tail vein puncture before and 60, 120, 180, and 240 min after T_3 injection.

Indirect Calorimetry and Activity. Food intake, VO_2, CO_2 production (VCO_2), respiratory exchange ratio (VCO_2/VO_2); and locomotor activity were assessed using a combined indirect calorimetry system (TSE Systems). After 2–3 h of adaptation, VO_2 and VCO_2 were measured every 15 min for a total of 21 h. Food intake was determined continuously for the same time as the indirect calorimetry assessments by integration of scales into the sealed cage environment. Locomotor activity was determined using a multidimensional infrared light beam system and was expressed as the distance traveled (in centimeters) per 15-min period. Differences in VO_2 between groups were evaluated using linear regression models including body mass as a covariate.

Thyroid Function Tests and Analysis of Serum Parameters and Triglyceride Concentration. Blood was collected by cardiac puncture. Serum TSH was measured with a sensitive, heterologous disequilibrium double-antibody precipitation RIA (40). Results are expressed in milliunits per liter. Serum total T_4 and total T_3 concentrations were measured by RIA (DRG Instruments) following the manufacturer's instructions. Thirty microliters of serum were used to analyze triglycerides, cholesterol, albumin, and total protein on an ADVIA 2400 Chemistry System (Siemens Healthcare). Blood glucose concentration was measured with a Contour XT glucometer (Bayer). Fifty milligrams of shock-frozen liver tissue were homogenized in 300 μL PBS with 1% Triton X-100. Lysates were boiled for 10 min at 95 °C, and the supernatant was collected after 10 min of centrifugation with 17,000 × *g*. Whole lysates were used for triglyceride measurement with an ADVIA 2400 system.

Oil Red O Staining. Livers were embedded in Tissue-Tek O.C.T compound (Sakura Finetek) and were shock-frozen in the gas phase of liquid nitrogen. Five-microliter sections were fixed in 10% formalin for 30 min at RT. Oil red O working solution consisted of three parts 0.3% Oil red O stock solution (in 99% isopropanol) and two parts deionized water. Sections were preincubated with 60% isopropanol for 5 min at RT, followed by incubation in Oil red O working solution for 15 min. After rinsing with tap water, sections were counterstained with hematoxylin and were covered immediately. Stained sections were imaged on the day of staining.

ChIP. ChIP was performed as previously described (42) with the following modifications. Twenty-five milligrams of frozen liver tissue were used per immunoprecipitation. The procedure was performed on whole-cell material or isolated nuclei involving 1.5-h incubation in lysis buffer 1 [1% SDS, 20 mM EDTA, 50 mM Tris·HCl (pH 8.0), 1 μg/μL BSA, and proteinase inhibitors]. Samples were resuspended in lysis buffer 2 [0.1% SDS, 1% Triton X-100, 150 mM NaCl, 1 mM EDTA, 20 mM Tris·HCl (pH 8.0), 1 μg/μL BSA, and proteinase inhibitors] and were sonicated using a Diagenode Bioruptor Twin or Covaris ME220 ultrasonicator. Immunoprecipitations using 0.2 or 1 μg antibodies against H3K27Ac (ab4729; Abcam), RXRα D-20 (sc-553; Santa Cruz), or TR (12) were performed with overnight incubation followed by 2-h incubation with 30 μL Protein A/G PLUS-Agarose beads (sc-2003; Santa Cruz). Beads were extensively washed, and DNA–protein complexes were isolated with elution buffer (1% SDS and 0.1 M $NaHCO_3$). DNA–protein complexes were decrosslinked at 65 °C for at least 6 h, and DNA was purified by phenol/chloroform extraction. Enrichment of TR, RXR, and H3K27Ac at specific TR-binding sites was evaluated by qPCR using the following primer pairs: negative control site F: 5′-TGGTAGCCTCAGGAGCTTGC-3′, R: 5′-ATCCAAGATGGGACCAAGCTG-3′; *Dio1* +7.0 kb F: 5′-CAGGCAAAGGGAGTCAATGT-3′, R: 5′-GGTTCCGGACAGTGGTCTTA-3′; *NCoR2* +22.4 kb F: 5′-AGGCGGTGTCTGTACTCCTG-3′, R: 5′-CACTAGGCACCAGAGGGAAG-3′; *H13* +3.1 kb F: 5′-GGGAGTGTCCGAAACCTGTA-3′, R: 5′-CTGAAGCGAAAGCCCAATAG-3′; and *Strbp* +59.1 kb F: 5′-TTGCATCATGCTCAGTCAAA-3′, R: 5′-TGAATGCTCAGGGTCAGATG-3′.

Illumina Sequencing and Data Analysis. H3K27Ac ChIP-seq libraries were constructed using the NEBNext DNA Library Prep Kit according to the manufacturer's instructions (New England Biolabs). Sequencing was carried out on a HiSeq 1500 platform (Illumina). Sequenced tags were aligned to mm9 using STAR (45). Aligned tags were quantified at previously identified DNase-accessible regions in liver tissue (12) using HOMER (46). Differentially regulated H3K27Ac in the liver from WT animals in response to T_3 was identified by DESeq2 at a false-discovery rate (FDR) <0.1 and a log2 fold change greater than 1 or less than −1 (47). The heat map was generated using the pheatmap package in R using hierarchical clustering (48). These data have been deposited in the NCBI GEO database (43) with the GEO Series accession no. GSE104877.

Gene-Expression Analysis. Total RNA was isolated from liver and heart (RNeasy Kit; QIAGEN) and stored at −80 °C. Two micrograms of total RNA were reverse transcribed into cDNA with SuperScript III (Invitrogen) and random hexamer primers. qRT-PCR was performed using Roche SYBR Green I Master Mix on a LightCycler LC480 (Roche). Please see Dataset S1 for primer sequences. In compliance with the Minimum Information for Publication of Quantitative Real-Time PCR Experiments (MIQE) guidelines for qRT-PCR (41), we used a set of three reference genes per tissue for accurate normalization and calculation (liver: *18S*, *Ppia*, and *Rpl13a*; heart: *18S*, *Gapdh*, and *Hprt1*). Ct values <35 were used for analysis and calculation of the fold change in gene expression by the efficiency-corrected method (49). For microarray analyses, we used the Affymetrix GeneChip platform employing the Express Kit protocol for sample preparation and microarray hybridization. Total RNA (200 ng) was converted into biotinylated cRNA, purified, fragmented, and hybridized to MG-430_2.0 microarrays (Affymetrix). The arrays were washed and stained according to the manufacturer's recommendation and finally were scanned in a GeneChip 3000 scanner (Affymetrix). Array images were processed using Partek Genomics Suite software [Robust Multi-array Average (RMA) algorithm]. Differentially expressed probe sets were identified using the implemented ANOVA method and the step-up procedure to correct for multiple testing. The data discussed in this publication have been deposited in the NCBI GEO database (43) with GEO Series accession number GSE93864.

Bone Histology. Tibias were fixed in 10% neutral-buffered formalin and decalcified in 10% EDTA, embedded in paraffin wax. Sections (5 μm) were stained with Alcian blue and van Gieson stains (18). To calculate the mean height, measurements from at least four separate positions across the growth plate were

obtained using a Leica DMLB2 microscope and DFC320 digital camera (Leica Microsystems). Results from two levels of sectioning were compared.

Faxitron Digital X-Ray Microradiography. Femurs were imaged at 10-μm resolution using a Faxitron MX20 unit (Qados). Bone mineral content was determined relative to steel, aluminum, and polyester standards. Images were calibrated with a digital micrometer, and bone length was determined (18, 19).

Micro-CT. Femurs were imaged by micro-CT (Scanco μCT50; Scanco Medical AG) at 70 kV, 200 μA with a 0.5-mm aluminum filter and a voxel resolution of 3 μm. Images were reconstructed and analyzed using Scanco software. A 1-mm^3 region of interest was selected 100 μm from the growth plate, and trabecular bone (BV/TV), trabecular number (Tb.N), and trabecular thickness (Tb.Th) were determined (18). A 1-mm region of interest centered in the midshaft 56% along the length of the femur distal to the femoral head was used to determine cortical area (Ct.Ar), cortical thickness (Ct.Th), and cortical bone mineral density. Raw data [333 cross-sections per specimen in 450 × 450 pixel 16-bit Digital Imaging and Communications in Medicine (DICOM) files] from representative femurs from each genotype were imported using 32-bit Drishti v2.0.221 (Australian National University Supercomputer Facility, anusf.anu.edu.au/Vizlab/drishti/) and were rendered using 64-bit Drishti v2.0.000 to generate high-resolution images.

Immunoblotting. Whole-protein lysates were generated from snap-frozen liver tissue homogenized in RIPA buffer (150 mM NaCl, 50 mM HCl, 1% Nonidet P-40, 0.5% sodium deoxycholate, 0.1% SDS, 2 mM EDTA, 50 mM NaF) with cOmplete protease inhibitor (Roche). After 30-min incubation on ice with gentle agitation, lysates were sonicated with an ultrasound probe (Sonoplus). After 10 min of centrifugation with 17,000 × *g* at 4 °C, the supernatant was collected, and the cell debris was discarded. Twenty micrograms of the samples were separated by SDS/PAGE and transferred to a PVDF membrane (Roti-Fluoro PVDF; Roth). After blocking with 5% milk in TBS-T (Tris-buffered saline with 0.5% Tween-20) for 1 h, membranes were incubated for 16 h at 4 °C under gentle agitation with the desired primary antibody against *Scd1* (SCD H-300, sc-30081; Santa Cruz), *Me1* (PA5-21550; Thermo Fisher Scientific), *Fasn* (MA5-14887; Thermo Fisher Scientific), and *Gapdh* (ACR001P, Acris Antibodies). Horseradish peroxidase-labeled secondary antibody against rabbit IgG and Alexa-Fluor 488-labeled antibody against mouse IgG (goat anti-mouse IgG DyLight488; Thermo Fisher Scientific) were used in an appropriate dilution for detection with a VersaDoc MP 4000 system (Bio-Rad).

Ex Vivo Heart Rate in Isolated Perfused Hearts. Isolation and cannulation of hearts were performed in a Langendorff apparatus as previously described (50). Briefly, at a constant pressure of 80 mm Hg, hearts were perfused with modified Krebs–Henseleit buffer (118 mM NaCl, 4.7 mM KCl, 1.64 mM $MgSO_4 \times 7\ H_2O$, 0.02 g/L EDTA, 2 mM Na-pyruvate, 1.18 mM KH_2PO_4, 5.55 mM glucose, 24.88 mM $NaHCO_3$, and 2 mM $CaCl_2$). A water-filled balloon made from saran wrap (Toppits; Cofresco Frischhalteprodukte GmbH & Co. KG) was inserted through the mitral valve into the left ventricular cavity and connected to a pressure transducer (DPT-6000 Pvb; Codan) to allow continuous monitoring of left ventricular pressure. Based on the cyclic measurements of the LV pressure waves, the LabChart software (ADInstruments) allows continuous measurement of the heart rate. After 10 min the basal ex vivo heart rate was recorded for 1 min, and the mean heart rate was calculated.

Statistics. We used one-way ANOVA with Tukey's post hoc test for statistical analysis for normally distributed datasets unless otherwise noted. Differences were considered significant when $P < 0.05$. For gene-expression data, statistical significance was calculated on log-transformed data (to obtain normal distribution) as recommended by the MIQE guidelines (41). Data were analyzed and plotted with GraphPad Prism 6 (GraphPad Software).

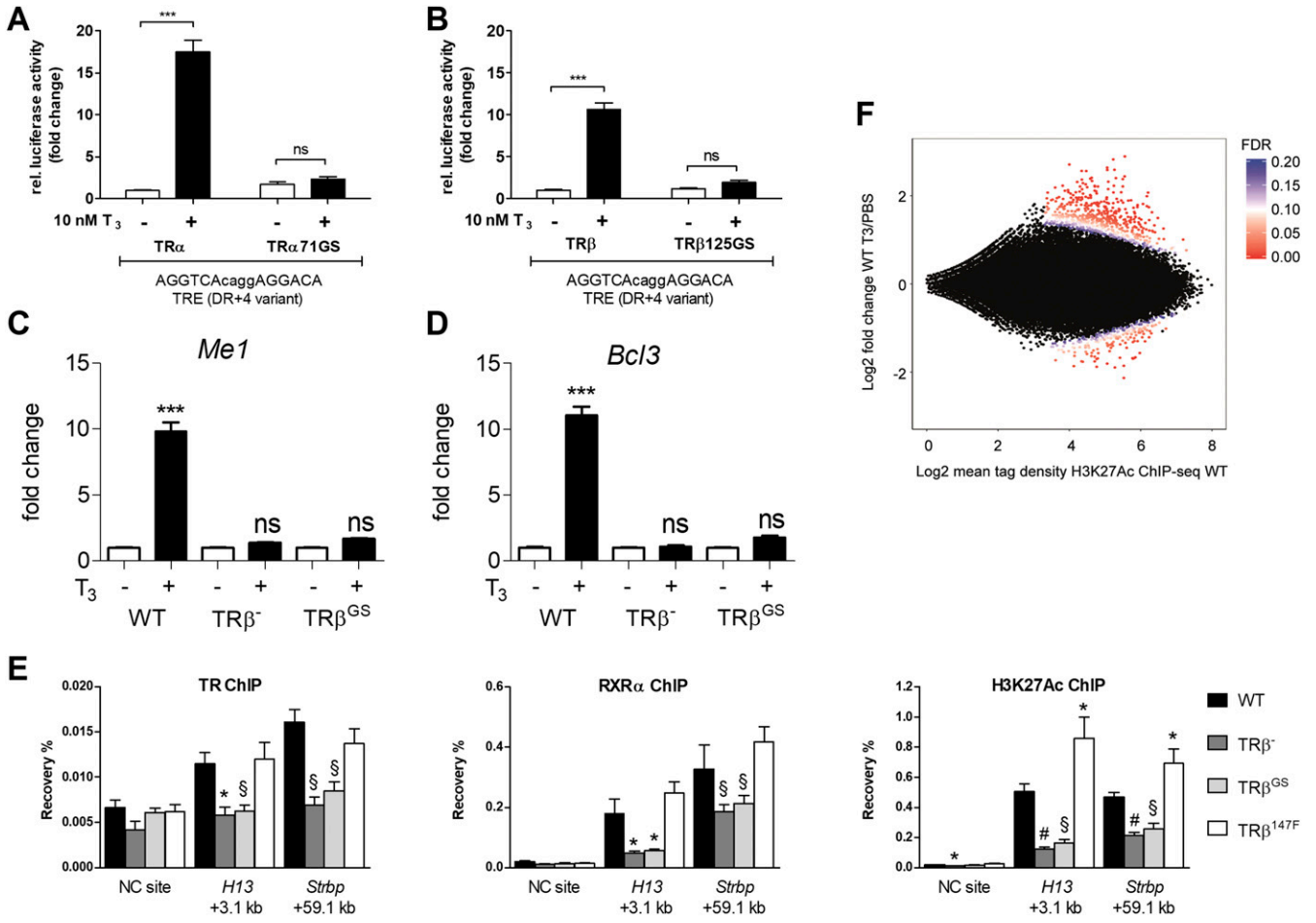

Fig. S1. The GS mutation mediates abrogation of DNA binding and canonical action of TRs. (*A* and *B*) HEK293 cells transfected with plasmids encoding for TRβ and TRβ125GS (*A*) and TRα and TRα71GS (*B*) and a luciferase reporter plasmid under the control of an alternative DR+4 sequence. Cells were treated with 10 nM T_3 for 48 h (black bars) to induce luciferase expression via canonical TR/TRE-mediated action for TRα and TRβ variants. Data are shown as mean ± SEM; ANOVA and Tukey's post hoc test; ns, not significant, $^{***}P < 0.001$. (*C* and *D*) Response of TH target genes *Me1* (*C*) and *Bcl3* (*D*) to T_3 in livers of hypothyroid WT, $TR\beta^{-}$, and $TR\beta^{GS}$ mice. Hypothyroid mice were injected with either vehicle (open bars) or with T_3 at 50 ng/g BW (black bars) for four consecutive days; $n = 6$. Data are shown as mean ± SEM; ANOVA and Tukey's post hoc test; ns, not significant, $^{***}P < 0.001$. (*E*) ChIP of H3K27Ac, RXRα, and TRβ was followed by qPCR to determine H3K27Ac and recruitment of RXRα and TR to TR-binding sites located +3.1 kb and +59.1 kb from the transcriptional start site of *H13* and *Strbp* of T_3-treated $TR\beta^{-}$, $TR\beta^{GS}$, and $TR\beta^{147F}$ mice compared with WT mice; $n = 4$–6 mice per genotype. Data are shown as mean ± SEM; Student's *t* test; $^{*}P < 0.05$, $^{\#}P < 0.005$, $^{\S}P < 0.001$). (*F*) H3K27Ac ChIP-seq experiments were performed using livers from hypothyroid WT mice treated with PBS or T_3 for 6 h. H3K27Ac was quantified at 79,938 DNase-accessible regions previously identified in mouse liver tissue. A total of 537 DNase-accessible regions showed differential H3K27Ac at an FDR <0.1 and a log2 fold change of least 1; $n = 2$.

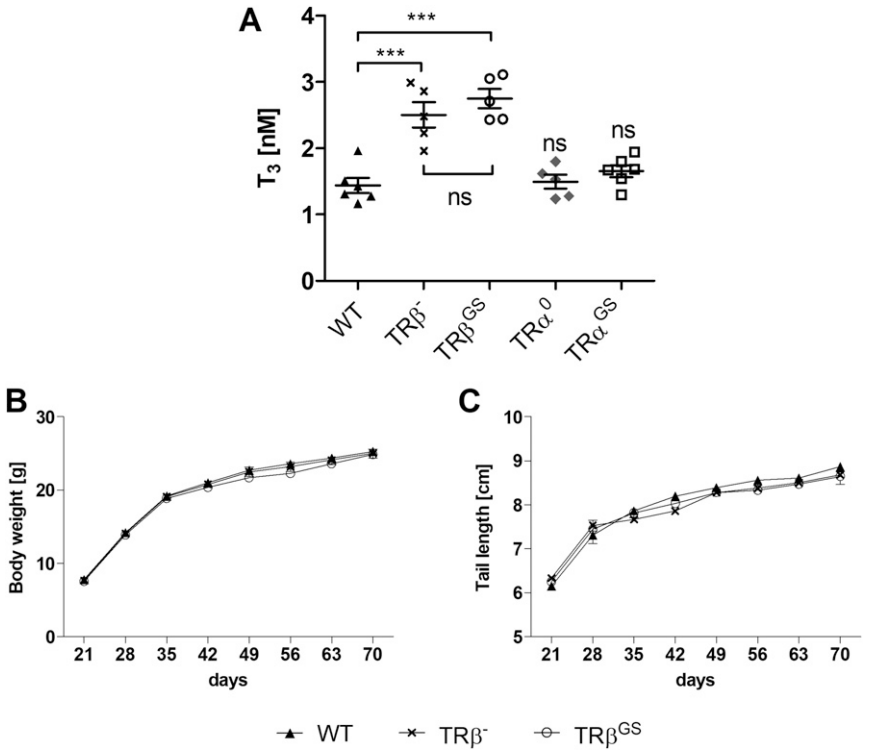

Fig. S2. Serum T_3 concentrations and growth curves of TRβ-mutant mice. (*A*) T_3 in serum of 15-wk-old WT (black triangles; $n = 11$) TRβ$^-$ (**x**; $n = 9$), TRβ^{GS} (open circles; $n = 10$), TRα^0 (gray diamonds; $n = 5$), and TRα^{GS} (open squares; $n = 6$) male mice. Data are shown as mean ± SEM; ANOVA and Tukey's post hoc test; ***$P < 0.001$; ns, not significant. (*B*) Mice were weighed once a week to monitor gain of body weight; $n = 6$ or 7 mice per genotype. Data are shown as mean ± SEM; ANOVA with Tukey's post hoc test. (*C*) Linear growth was determined by weekly measurements of tail length.

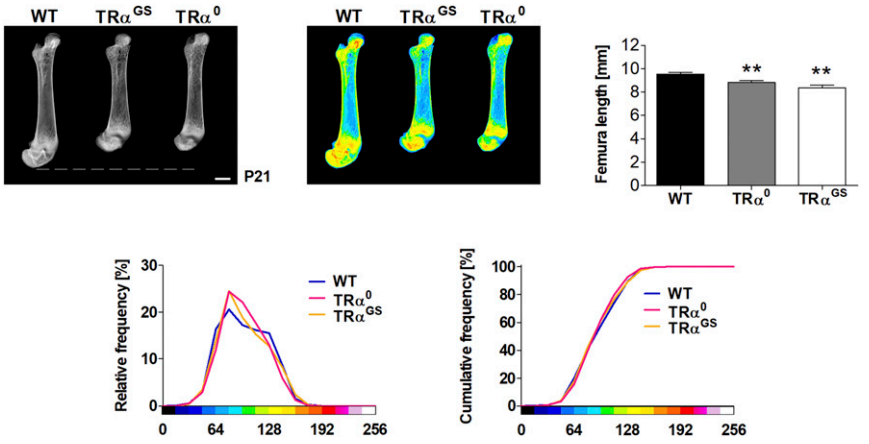

Fig. S3. Canonical TRα action is necessary for normal development of long bones of mice at P21. (*Upper*) Gray-scale images (*Left*) of femurs from P21 WT ($n = 5$), TRα^{GS} ($n = 5$), and TRα^0 ($n = 3$) mice were pseudocolored (*Middle*) according to a 16-color palette in which low mineral content is blue and high mineral content is red. (Scale bar: 1,000 μm.) (*Right*) The graph demonstrates femur length of WT (black bar), TRα^{GS} (gray bar), and TRα^0 (open bar) mice. Data are shown as mean ± SEM; ANOVA and Tukey's post hoc test; **$P < 0.01$. (*Lower*) Relative (*Left*) and cumulative (*Right*) frequency histograms display bone mineral content of femurs from TRα^{GS} and TRα^0 vs. WT mice; Kolmogorov–Smirnov test, not significant.

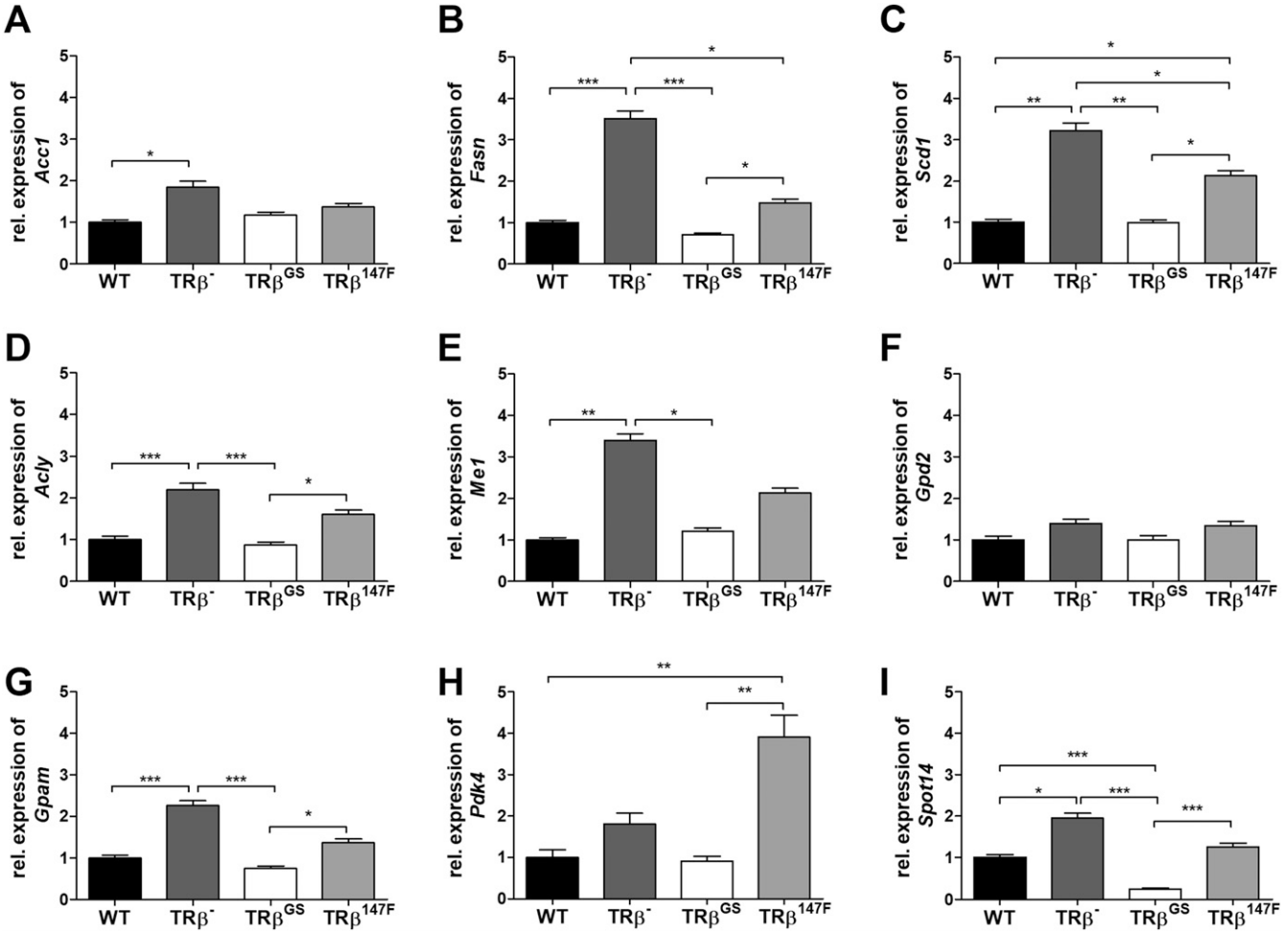

Fig. S4. Hepatic mRNA expression profile of key enzymes and regulatory proteins involved in triglyceride synthesis. (*A*–*G*) mRNA expression of enzymes involved in TG synthesis in livers of WT (black bar), $TR\beta^{-}$ (dark gray bar), $TR\beta^{GS}$ (open bar), and $TR\beta^{147F}$ (light gray bar) mice: acetyl-CoA carboxylase (*Acc1*) (*A*), fatty acid synthase (*Fasn*) (*B*), Δ9-steaoryl-CoA desaturase (*Scd1*) (*C*), ATP-citrate lyase (*Acly*) (*D*), malic enzyme (*Me1*) (*E*), glycerol-3-phosphate dehydrogenase (*Gpd2*) (*F*), and mitochondrial glycerol 3-phosphate acyltransferase (*Gpam*) (*G*). (*H* and *I*) mRNA expression of proteins regulating fuel demand (pyruvate dehydrogenase kinase 4; *Pdk4*) (*H*) and lipogenesis (thyroid hormone responsive; *Spot14*) (*I*); $n = 4$–6 mice per genotype; ANOVA with Tukey's post hoc test on log-transformed qRT-PCR data; $^{*}P < 0.05$; $^{**}P < 0.01$; $^{***}P < 0.001$.

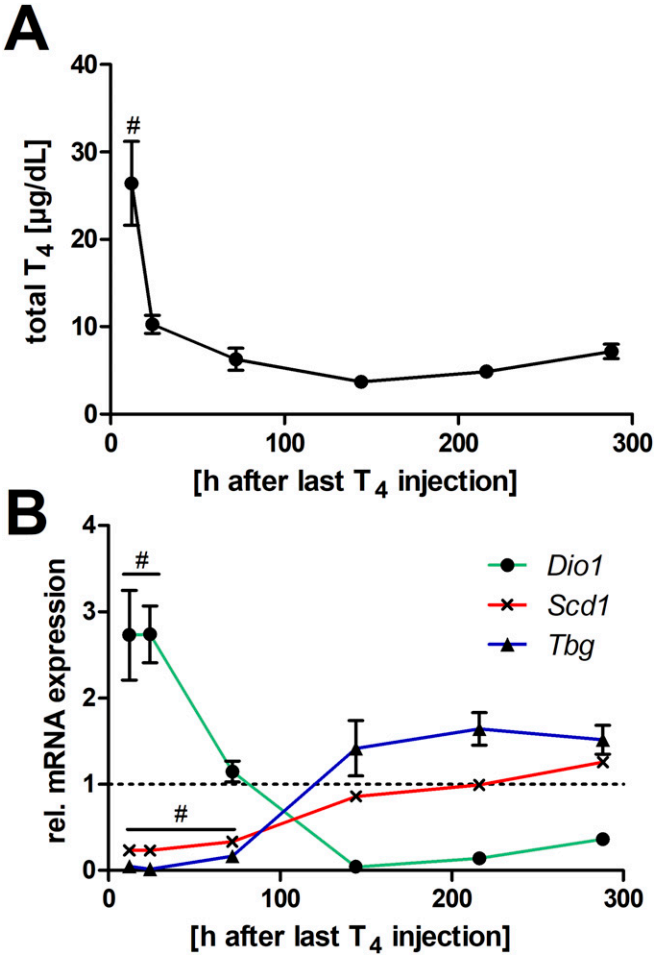

Fig. S5. Time course of T_4 serum concentration and hepatic TH target gene expression. (*A*) T_4 serum concentration of hyperthyroid mice (i.p. injection of T_4 1,000 ng/g BW every other day for 6 wk) was measured at the indicated time points after the last injection. (*B*) Hepatic TH target gene expression: *Dio1* followed the T_4 kinetics, whereas the negatively regulated TH target genes thyroxine binding globulin (*Tbg*) and Δ9-steaoryl-CoA desaturase (*Scd1*) showed a negative correlation with T_4 serum concentrations; $n = 5$–6 mice per condition. Data are shown as mean ± SEM; ANOVA followed by Tukey's post hoc test; $^{\#}P <$ 0.001 compared with untreated mice.

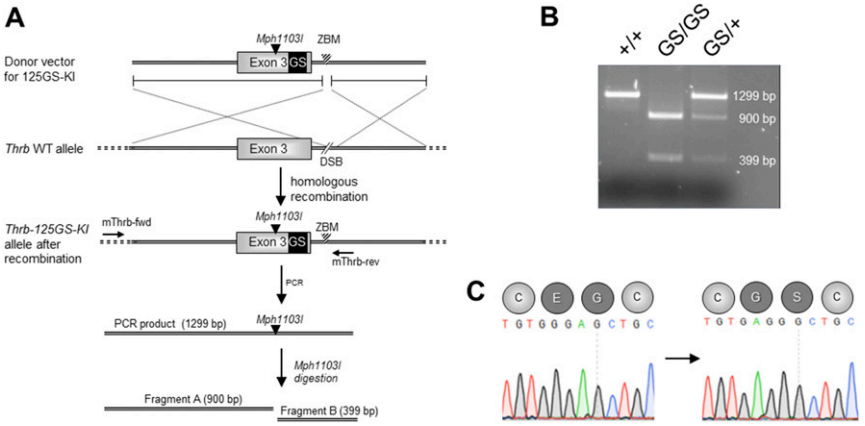

Fig. S6. Generation of $TR\beta^{GS}$ knockin mice. (*A*) A donor vector containing the desired point mutations and ZFN mRNA were microinjected into the pronucleus of an oocyte. A zinc finger-binding mutation (ZMB) was introduced into the donor vector sequence to protect it from ZFN. The genomic WT allele was cut by ZFN, and the double-strand break (DSB) was repaired by homologous recombination using the donor vehicle sequence as a template. In addition to the point mutations leading to the amino acid exchange from EG to GS, a silent mutation was introduced to generate an Mph1103I restriction site to facilitate genotyping by RFLP-PCR. Positive founder animals were identified with RFLP-PCR using a forward primer (ThrbGS-fwd), which binds to a sequence of the *Thrb* gene outside the left homologous sequence of the donor vehicle, and a reverse primer (ThrbGS-rev) located downstream of exon 3. (*B*) Restriction enzyme digestion of the PCR product revealed homo- and heterozygosity for the mutated allele. (*C*) Integration of the GS mutation was confirmed by sequencing. $TR\alpha^{GS}$ mice were generated in parallel using the same techniques.

Table S1. Absolute blood glucose concentrations (mg/dL) before and 60 min after T_3 injection

Genotype	Before T_3	60 min after T_3	$\Delta\bar{x}$	Δ%
WT	179 ± 40	127* ± 6	−52	−29
TRβ^{-}	150 ±17	151 ± 21	+1	+0
TRβ^{GS}	137 ± 26	102* ± 10	−35	−26
TRβ^{147F}	158 ± 12	158 ± 12	+0	+0

Values are shown as mean ± SD; n = 4–5 mice per genotype.
*$P \leq 0.02$, paired Student's t test.

Table S2. Serum parameters

Parameter	WT	TRβ^{-}	TRβ^{GS}	TRβ^{147F}
Total protein, g/dL	6.0 ± 0.0	6.3 ± 0.3	5.8 ± 0.2	5.9 ± 0.3
Albumin, g/dL	3.4 ± 0.2	3.7 ± 0.2	3.6 ± 0.2	3.6 ± 0.2
Cholesterol, mg/dL	134.0 ± 10.8	163.3 ± 15.2	146.0 ± 3.3	155.2 ± 13.4

Values are shown as mean ± SEM; n = 6; one-way ANOVA; Tukey's post hoc test.

Table S3. Indirect calorimetry of TRβ^{-} and TRβ^{GS}

	Female		Male		Linear model	
	Control, n = 10	Mutant, n = 10	Control, n = 10	Mutant, n = 10	Genotype	Body weight
TRβ^{GS}						
Avg body weight, g	19.4 ± 1.1	19.6 ± 1.4	25.7 ± 1.7	24.9 ± 1.8	P = 0.506	NA
Food intake, g	2.2 ± 0.6	2.2 ± 0.9	2.5 ± 0.4	2.7 ± 0.6	P = 0.812	P = 0.682
Avg. VO_2, mL·h^{-1}·animal^{-1}	80.2 ± 6.8	81.6 ± 6.2	80.9 ± 6.7	86.3 ± 10.0	**P = 0.041**	**P < 0.001**
Minimum VO_2, mL·h^{-1}·animal^{-1}	59.1 ± 7.1	56.5 ± 7.8	57.9 ± 5.9	61.8 ± 8.7	P = 0.477	**P = 0.002**
Maximum VO_2, mL·h^{-1}·animal^{-1}	109.1 ± 7.18	109.3 ± 6.5	111.8 ± 13.1	121.0 ± 12.4	**P = 0.032**	**P < 0.001**
TRβ^{-}						
Avg. body weight, g	20.4 ± 0.8	19.6 ± 1.8	27.4 ± 1.6	25.1 ± 1.5	**P = 0.003**	NA
Food intake, g	2.0 ± 0.5	2.1 ± 1.0	2.9 ± 0.8	2.1 ± 1.1	P = 0.491	P = 0.322
Avg. VO_2, mL·h^{-1}·animal^{-1}	82.1 ± 6.1	82.0 ± 4.9	90.8 ± 9.2	80.1 ± 6.8	P = 0.204	**P = 0.042**
Minimum VO_2, mL·h^{-1}·animal^{-1}	60.3 ± 6.2	61.5 ± 6.4	67.6 ± 10.0	55.8 ± 7.0	P = 0.259	P = 0.074
Maximum VO_2, mL·h^{-1}·animal^{-1}	111.6 ± 9.3	110.3 ± 7.1	124.9 ± 13.2	113.4 ± 9.6	P = 0.289	P = 0.126

Values are shown as mean ± SD; linear regression model; P < 0.05 was considered statistically significant (bold); Avg, average; NA, not applicable.

Other Supporting Information Files

Dataset S1 (DOCX)